



# Mechanism of cross-level settlements and void accumulation of wide and conventional sleepers in railway ballast

Olga Nabochenko<sup>1</sup> · Mykola Sysyn<sup>1</sup> · Norman Krumnow<sup>2</sup> · Szabolcs Fischer<sup>3</sup>

Received: 26 May 2023 / Revised: 27 December 2023 / Accepted: 1 January 2024  
© The Author(s) 2024

## Abstract

The cross-level and twist irregularities are the most dangerous irregularity types that could cause wheel unloading with the risk of derailments and additional maintenance expenses. However, the mechanism of the irregularities initiation and development is unclear. The motivation of the present study was the previous experimental studies on the application of wide sleepers in the ballasted track. The long-term track geometry measurements with wide sleepers show an enormous reduction of the vertical longitudinal irregularities compared to the conventional track. However, wide sleepers had higher twist and cross-section level irregularities. The present paper aims to explain the phenomenon by discrete element method (DEM) modeling the development process of sleeper inhomogeneous support at cross-level depending on the sleeper form. The DEM simulations show that the maximal settlement intensity is up to 3.5 times lower for a wide sleeper in comparison with the conventional one. Nevertheless, the cross-level differential settlements are almost the same for both sleepers. The particle loading distribution after all loading cycles is concentrated on the smaller area, up to the half sleeper length, with fully unloaded zones under sleeper ends. Ballast flow limitation under the central part of the sleeper could improve the resilience of wide sleepers to the development of cross-level irregularities. The mechanism of initiation of the cross-level irregularity is proposed, which assumes the loss of sleeper support under sleeper ends. The further growth of inhomogeneous settlements along the sleeper is assumed as a result of the interaction of two processes: ballast flow due to dynamic impact during void closing and on the other side high pressure due to the concentration of the pressure under the middle part of the sleeper. The DEM simulation results support the assumption of the mechanism and agree with the experimental studies.

**Keywords** Wide sleeper · Ballasted track · Sleeper support inhomogeneity · Sleeper foot form · Discrete element modeling · Void accumulation

## 1 Introduction

### 1.1 The experience of wide sleepers' application

Until now, there have been many attempts to improve the ballasted track behavior by the application of the slab and wide sleepers [1, 2]. The experimental studies to compare railway track sections with the same operation conditions

but with two different sleeper types (conventional sleepers B70 and wide sleepers BBS) were performed by German Railways in 1997–2000 and presented by Unbehaun [1]. Two railway track sections (Homburg–Neunkirchen/Saar and Bexbach–Neunkirchen) were investigated and measured over four years. Reference [1] describes the construction and arrangement of the railway section with wide sleepers in detail. A comparison of technical parameters between two applied sleeper types is presented below in Table 1.

The outline of a wide sleeper BBS with necessary geometrical parameters is depicted in Fig. 1, and the arrangement of the experimental section is shown in Fig. 2a.

The comparison of the measurement results of two railway sections with wide sleepers BBS and conventional sleepers B70 is described in Table 2. Notable is that in the longitudinal level wide sleepers BBS behave very stable, while in the cross-level direction, conventional sleepers B70

✉ Mykola Sysyn  
mykola.sysyn@tu-dresden.de

<sup>1</sup> Institute of Railway Systems and Public Transport, Technical University of Dresden, Dresden, Germany

<sup>2</sup> Rhomberg Sersa Deutschland GmbH, Berlin, Germany

<sup>3</sup> Central Campus Győr, Széchenyi István University, Győr, Hungary

**Table 1** Comparison of technical parameters of a wide sleeper (BBS) and a conventional sleeper B70 [1]

Comparison items	Sleeper B70	Wide sleeper (BBS)	Difference
Sleeper length (m)	2.60	2.40	-0.20 m
Sleeper width (m)	0.30	0.57	+0.27 m
Support area (cm <sup>2</sup> )	5700	10,260	+80%
Side area (cm <sup>2</sup> )	570	830	+45%
Own weight (kg)	320	560	+75%

work better. Concerning “twist” and “longitudinal level difference”, the results for conventional sleepers are about 8% lower. Railway track operation experience has shown that wide sleeper track geometry deteriorates extremely slowly; however, other railway track failures occur, even with higher irregularity values.

According to a relevant study [4], under a load of 20 million tons the settlements of railway tracks with the subgrade protection layer for wide sleepers (green line, Fig. 2b) are 21.8% lower than for conventional sleepers B70 (red line). As the loading increase, the difference in settlements tend to be slightly more significant. Without a subgrade protection layer, the values change significantly. Thus, the settlements of the railway section with wide sleepers (light green line, Fig. 2b) are 54.6% lower than with conventional sleepers B70 (light red line). During the last 5 million tons, a relatively large increase rate of settlements of a railway section with conventional sleepers B70 can be observed in comparison with those with wide sleepers.

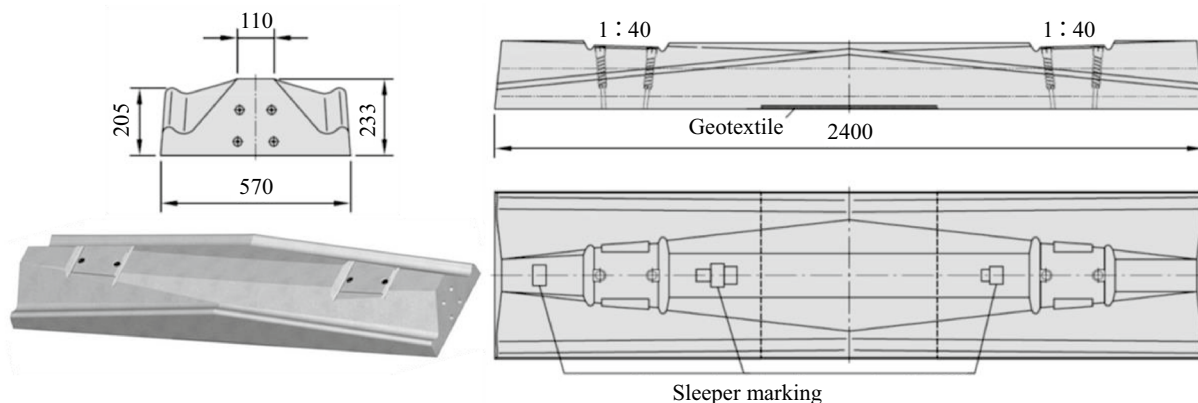
Another application of the wide or so-called “ladder sleeper”, a kind of longitudinal sleeper, is presented by Railway Technical Research Institute in Japan [2]. It had a “ladder” shape, in which both parallel longitudinal concrete beams were connected with steel pipe connectors. Thus, the central part of the ballast bed was not loaded. It was

expected that the ballasted ladder track would have much less deterioration caused by ballast wear. However, the structure has not found wide application over the last 20 years.

## 1.2 A problem of twisting and cross-level irregularities of railway track geometry

From the presented studies, it is clear that the wider sleeper has the advantage of lower longitudinal settlements, but it has a problem with twisting and cross-level irregularities. Cross-level and twisting are two indices of track geometry failures that appear due to differential settlements of the ballast layer. The differential settlement of the ballast layer along the sleeper or across the track axis causes the appearance of cross-level and twist irregularities of track geometry. The twist is defined in [5, 6] as the algebraic difference between two track cants taken at a defined distance apart, usually expressed as a gradient between the two points of measurement, i.e., expressed as a ratio (% or mm/m). Twist measurements are either taken simultaneously at a fixed distance, e.g., at a distance equivalent to the wheelbase, or computed from consecutive measurements of cant. Normally, the twist is measured on a 6-m base; i.e., the cant is measured at two points with a 6-m distance. The cant is expressed as the difference in elevation of the two rails; outside a curve, the cant should be zero. If the cant changes too rapidly, there appears the twist irregularity that causes a danger of derailment due to vehicle lateral oscillations and wheel unloading. The cross-level irregularities are the difference between the track cant and the design cant over a long distance. The irregularities do not cause safety issues, but they cause rail inhomogeneous overloading, increased wear, etc., which increases maintenance costs.

The importance of cross-level irregularities and their impact on railway operation are highlighted by many researchers [6, 7]. Three main reasons for twist occurrences have been mentioned, including cant change in the curve

**Fig. 1** Geometrical parameters of a wide sleeper BBS (unit: mm) [3]

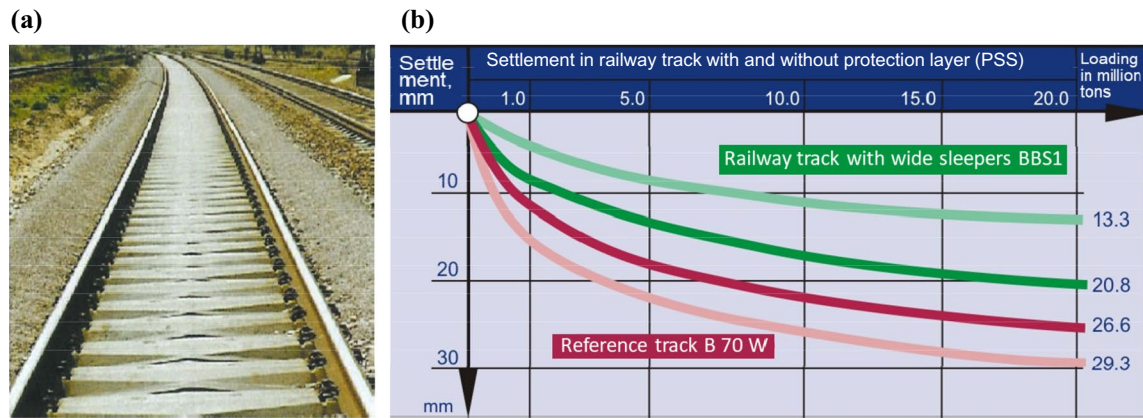


**Fig. 2** **a** Experimental section of the railway track with wide sleepers BBS [1] and **b** comparison of settlements of railway tracks with conventional and wide sleepers [4]

transition area, track fault, track repair works. In Ref. [6], it is emphasized that twist faults present a derailment risk to all traffic regardless of speed. During twist measurements, two values can be obtained: static and dynamic twists. A static twist can be measured with a cross-level gauge without vehicle loading, while a dynamic twist needs to be measured with train loading or when a track-measuring car passes. The measurement of static twists does not take into account voids of sleepers but void measurements are important to cross-level gauges when dealing with dynamic twists.

Also, Bergquista and Söderholm [7] investigated twist failures of tracks as one of the most concerned problem with track safety parameters. They processed observations of about 30 track geometry variables and presented two examples of control charts for plotting condition data, i.e., in the spatial and the spatiotemporal domains. The use of the control charts can optimize the track maintenance system as a consequence of statistically based alarm limits application instead of safety-related limits, which are connected with specifications.

However, the above studies have not presented the aspects of the track resilience to twist and cross-level failures.

**Table 2** Results of the 6 km measurement of the railway track with wide sleepers [1]

Parameter	Average values			Relative increase (%)
	B70	BBS	Difference	
Longitudinal level (mm)	18.7	6.8	+11.9	+175
Twist (mm/m)	19.6	21.9	-1.7	-7.80
Longitudinal level difference (mm)	11.7	21.9	-3.4	-7.90
Cross level irregularity (mm/m)	14.2	17.6	-3.4	-19.30
Overall assessment (mm)	21.5	16.1	+5.4	+33.5

### 1.3 Differential settlements of the ballast layer and void development

Geometric irregularities of rail tracks are typically caused by the differential settlements of the ballast layer that are frequently accompanied by the appearance of partially and fully unsupported sleepers or void zones in ballasted tracks. The loss of sleeper support under sleeper ends initiates twist and cross-level irregularities. The dynamic interaction in the sleeper-ballast bed contact accelerates the development of voids, which causes frequent maintenance works. The term “sleeper riding” (from the germ. Schwellenreiten) is often used in the maintenance practice of German railways to describe the phenomenon of inhomogeneous ballast support along the sleeper foot. Stibler [8] and Feurig [9] mentioned the effect of the phenomenon, but they did not study the process and the reasons for its appearance.

Lundqvist and Dahlberg [10] studied the ballast-sleeper impact because of unsupported sleepers by finite element (FE) simulation of several hanging sleepers with a void depth of up to 1 mm. The results show a growth of up to 70% in the sleeper-ballast force at the neighboring sleepers for a single-hanging sleeper with a 1 mm void. Nevertheless, the cross-level interaction of sleepers with ballast was not considered in their study.

A wide-ranging study on the sleeper void short- and long-term dynamic behavior is shown in [11]. The FE simulations with the constitutive model of hypo-plasticity allow long-term settlement prediction of the development of hanging sleepers. The factors of the ballast loading and vibrations were considered, and the phenomenological settlement equation was suggested. An experimental investigation by Zhu et al. [12] presents a 1:5 scale laboratory model and a numerical simulation model, which were used to study the dynamic behavior of unsupported sleepers. Both experimental and simulation results demonstrate the growth in the dynamic

interaction due to the unsupported sleepers. The studies also considered the void development along the track.

Bezin et al. [13] suggested a track model with unsupported sleepers using multibody system modeling and finite element method. The influence of the unsupported sleepers was considered in the simulation of the ballast–sleeper interaction through a bilinear function. The model simulated the vibrations due to hanging sleepers on the vehicle and the track; however, the impact of the sleeper on the ballast bed was not analyzed.

Recuero [14] proposed a finite-element track model for nonperiodic and asymmetrical mechanical defects. The model considers the unsupported sleepers using the nonlinear multibody railroad vehicle model. It was found that the wheel–rail contact forces have an up to 30% increase at higher speeds due to hanging sleepers. However, the process of impact interaction due to void closing was not explicitly considered in the study.

Zhu et al. [15] presented a multibody vehicle–track model assembly that couples the continuous and discrete systems. The simulation model considers an uncontacted spring–damping element underneath the voided sleeper and triangularly unsupported sleepers. The existence of a critical gap size that causes the largest force was concluded. Its depth was estimated at 2.5 mm for four unsupported sleepers. The wheel–rail contact loadings due to triangular supported sleepers were analyzed in detail, but the ballast loadings were not considered.

By using numerical simulations, Li et al. [16] studied the influence of the number and distribution of unsupported sleepers along the track structure. They considered the cases of a normal sleeper, a single unsupported sleeper, two continuous unsupported sleepers, and two interval unsupported sleepers. The results show that the impact of two continuous unsupported sleepers is considerably higher than that in the other two cases.

#### 1.4 Analysis of the influence of the sleeper support conditions

Many studies consider sleeper support conditions during track and vehicle interaction calculations [17, 18]. The results of a study by Sysyn et al. [18] indicate a dramatic increase in the ballast settlement intensity of the unsupported sleepers compared to the normally supported ones due to the impact in void closing. The mechanism of the impact and the influencing factors are analyzed. Nonetheless, the partial sleeper support and differential settlements across the track have not been considered.

In another study, Sysyn et al. [19] presented the dynamic behavior of railway tracks with sleeper voids in the ballast pulverization zone. The evaluation of experimental data has shown a dynamic impact in voided zones, which appears due

to the closure of the voids under the sleeper during the wheel passing in the voided zone. Also, the authors suggested a practical method for quantitative determination of the void features. However, the measurement of sleeper voids was not considered along the track.

Practical detection and quantification of sleeper voids is not a trivial task, which requires both manual and train loading measurements with further analysis. Sysyn et al. [17] provided an approach for the identification of sleeper support conditions and the development of methods that allow to differentiate between the void and geometrical irregularity based on track-side and on-board measurements.

Kim et al. [20] conducted theoretical and experimental research on the dynamic behavior of hanging sleepers. They proposed a method for unsupported sleeper identification using a falling weight deflectometer and simulated different loading patterns of fully supported and unsupported sleepers using the discrete element modeling technique.

Besides, a numerical model and experimental measurements of the dynamic loads on the ballast caused by trains passing a transition zone with hanging sleepers are presented in [21]. The results show that the forces on the ballast have undergone significant variation in time and location of a transition zone due to the presence of voids under the sleepers. Yet, the interaction in the void zone was considered in the longitudinal plane. Zuada and Hicks [22] made a performance assessment of a transition zone with unsupported sleepers using numerical analysis. They identified a critical train speed in the transition zone and analyzed the stress redistribution toward the free ends of the void zones. Paixão et al. [23] demonstrated a parametric study with nonlinear dynamic analyzes using an FEM model of the track with unsupported sleepers. The unsupported sleepers were found strongly related to critical situations of track degradation. Nevertheless, ballast dynamic loadings were not considered. Mosayebi et al. [24] observed the impact of the void under an unsupported sleeper on the sleeper displacement and track support loading. As a result, a series of regression equations were derived for the maximal particle velocity in the surrounding environment of a railway track and the sleeper support stiffness for unsupported and fully supported sleepers.

Recently, the combined effect of supported and unsupported sleepers on the lateral ballast resistance in ballasted railway tracks was studied by Xu et al. [25] by conducting experiments on 1/5-scale ballasted track models. The results show that the lateral ballast resistance decreased significantly once a gap was generated between the bottom of the sleeper and the ballast, whereas the effect of the gap size on the lateral ballast resistance was insignificant.

Liu et al. [26] studied the influence of unsupported sleepers on the dynamic stability of ballasted beds based on wheelset impact tests. They investigated four different

conditions of hanging sleepers. The first-order rigid vibration mode at the frequency of 101 Hz is supposed to have a significant effect on the condition without unsupported sleepers. Additionally, the lateral stability of the hanging sleepers was studied. Still, the dynamic effects due to the impact of the sleeper foot on the ballast bed were not taken into account.

Zhang et al. [27] studied the detection of absent sleeper support in a ballasted track with the application of model-based and data-driven methods. A 47-degree-of-freedom multi-body subsystem was used to generate data for the statistical learning of a three-layer convolutional neural network. The model was validated with experimental measurements.

Using the discrete element method (DEM), Balamonica et al. [28] revealed a frequency dependency of dynamic stiffness of the ballast used by the Swiss Federal Railways. The ballast dynamic stiffness is determined through impact experiments. The ballast dynamic stiffness shows a steady increase with frequency, particularly above 100 Hz, and is influenced by the preload. The results could be potentially useful for the simulation of impact interaction in zones of unsupported sleepers.

Fang et al. [29] developed a dynamics analysis framework combining the DEM and the multi-body dynamics method (MBD). The model is used to simulate dynamic responses of the locomotive and ballasted tracks considering 0–5 unsupported sleepers. Simulations show that the acceleration of wheelsets begins to increase when running to the position in front of the hanging area and increases to the maximum when running to the edge of this area. This effect was also experimentally measured and theoretically substantiated by the simulations in [17–19]. Nevertheless, the model does not explicitly present the impact on the hanging sleepers of the ballast bed due to the void closing.

The presented review of the numerous studies on track behavior with unsupported sleepers highlights the importance of the problem. Heretofore, most models present as a simple imitation of short-time dynamic interaction, few studies have presented the effect of varying void along the sleeper or the partially unsupported sleeper, and no study has presented and analyzed the long-term processes of the void accumulation along the sleeper and the corresponding cross-level irregularity.

The differential settlements across the track have a relation to the sleeper size and form. DEM is usually used for the simulation of the behavior of the ballast layer. Guo et al. [30] presented the discrete element modelling of railway ballast during the direct shear test. The model considers particle shape and rolling resistance by using the rolling resistance linear model and the linear contact model. Their another study [31] indicates the importance of the DEM model calibration under the aspects of particle morphology,

degradation, and contact model. DEM simulations are generally computationally expensive and can only be limited used for the simulation of long-term processes of ballast settlement accumulation. Therefore, the ways to improve the computational performance are important. Reference [31] claims that efficient DEM simulations of railway ballast are possible using simple particle shapes. However, accurate simulation demands proper model calibration. Reference [32] presents the shakedown behavior of railway ballast under cyclic loading. The model takes into account real particle shapes, vibration loading, loading amplitude, confining pressure, and particle breakage. However, both the number of particles in the tri-axial test and the loading cycles are relatively low to describe the long-term behavior of the ballast in track.

### 1.5 Sleeper shape influence and discrete element modeling for ballast layer

Many papers indicate that the shape and form of sleepers are very important for railway track behavior. Several scholars investigated sleeper shape in the context of track irregularities appearance. In Ref. [33], Boroujeni et al., with the help of DEM, calculated the lateral resistance of ballasted railway tracks with different sleepers and under different support conditions. They compared the lateral resistance of experimental test and DEM simulation for four sleeper types: B70, HA110, winged, and middle-winged sleeper at 2 mm displacement. There were four variants of support conditions: full support, lack of rail seat support, lack of center support, and high center binding condition. In comparison with B70 sleepers, the other three sleeper types have shown better results, from a 22% to 45% increase in lateral resistance. For example, the lack of center support is similar to conditions after tamping works. In this case, the winged sleeper had the best simulation results in providing lateral resistance. The authors also considered the presence of a crib and shoulder ballast. Analysis of calculations shows that the shape and support conditions of both sleepers significantly influence the lateral resistance. According to the results, full support conditions provide the best force distribution and lateral resistance, because the majority of ballast particles contact with the sleeper bottom.

Chalabii et al. [34] presented the optimal shape design of concrete sleepers under lateral loading using DEM simulation. The authors analyzed fourteen sleeper shapes by an optimization algorithm connected to the simulation model. They examined the effect of the weight of sleeper B70 on lateral resistance. Almost a 25% increase in lateral resistance is claimed to be reached due to the optimization. A similar study [35] presents the estimation of the effect of sleeper bottom texture on lateral resistance by using discrete element modeling. The results indicate a 32% increase in the lateral resistance due to the enhanced interaction between sleeper

and ballast particles. Both studies consider short-term processes of sleeper motion in the ballast layer.

A parametric study [36] of different shapes of concrete and composite sleepers resting on four different types of support was performed to understand which shape works best with each of the different support conditions. The sleeper performance was evaluated for the least differential deflection and pressure, considering the volume of material used and the lowest range of bending moments present. The results show that the overall differential deflection was greater for the composite sleepers than for concrete, but greater improvements were observed for the optimized composite sleeper shapes.

Reference [37] presents an investigation on the influence of sleeper shape and configuration on track–train dynamics. Several cases of dynamical problems, where elastically supported beams are excited by a moving concentrated force, are considered. It is concluded, based on the vertical displacements of rails, that the “Y”-type track shows one of the advantages of the track with “Y”-type sleepers as well as an advantage of double fasteners. However, only the short-time elastic interactions were considered, which could not give a conclusion about the track deterioration.

Reference [38] presents experimental and theoretical studies of the steel turnout sleeper. The reasons for sleeper defects of ballast void and low lateral resistance were studied using FEM, DEM, and modal analysis. The analysis shows that the characteristic frequencies of the sleeper are in the in-situ constraint condition range, which overlaps with the frequency range of track resonance. Additionally, the lower lateral resistance than that of conventional sleepers is concluded, but no long-term ballast settlement processes are considered.

The overall analysis of the studies on track geometry shows that cross-level failures cause the most unfavorable dynamic interaction compared to other irregularities, which could impact operational safety. The development of the cross-level irregularities depends on the loss of homogenous support along the sleeper and the formation of voids under sleeper ends. The experimental in-situ studies on wide-sleepers long-term measurements show that the wide sleeper is subjected to the same cross-level/twist development as the normal sleeper despite low average ballast pressure. Although many DEM and FEM studies have been conducted on railway ballast, no DEM study on twisting together with a wider sleeper was presented so far. It is important because the twisting partially originated from hanging; however, FEM or field tests cannot reveal its mechanisms.

## 1.6 Aim, task and relations of the research

The present paper aims to find out the explanation of the experimentally observed effect of quick irregularity growth

in the track cross-level for wide sleepers compared to the conventional sleeper foot form. The development of cross-level and twist irregularities is supposed to be related to the void development under the sleeper. The void development is accompanied by inhomogeneous loading of the ballast under the sleeper and impact interaction, which causes the accumulation of differential settlements along the sleeper. On the other side, the ballast layer under the central part of the sleeper and its ends have different confinement conditions for wide and conventional sleepers, resulting in different ballast flow and settlement accumulations. The supposed general relation between the sleeper form and track irregularities is presented in Fig. 3.

DEM simulations are used to explore the mechanism of inhomogeneous settlements of the ballast layer along the sleepers of two different forms under the combination of vertical homogenous and eccentric cyclic loadings. The analysis of the following simulation parameters is performed:

- (1) Long-term sleeper average settlements and sleeper inclination accumulation (differential settlements), sleeper settlement intensity, ballast particle stress evolution, ballast particle flow during whole loading cycles for two sleeper foot forms, and distribution of ballast layer porosity along the sleeper.
- (2) Short-time dynamic interaction for characteristic time moments in the loading history: in the beginning moment with good sleeper support, at the end of the simulation, and in zones (stable zone) of intensive settlement accumulation (unstable zone). The following dynamic parameters are analyzed:
  - Ballast particle loading process during the loading cycle, and sleeper vertical and angular acceleration.
  - Particle surface form under the sleeper foot and geometrical void distribution along the sleeper.

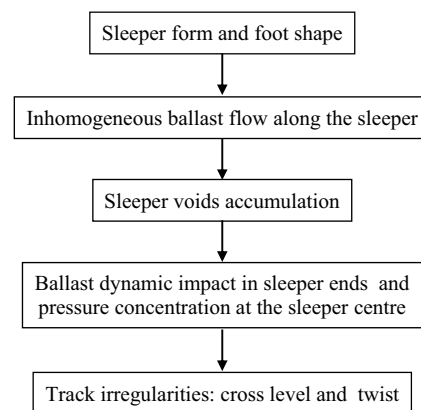
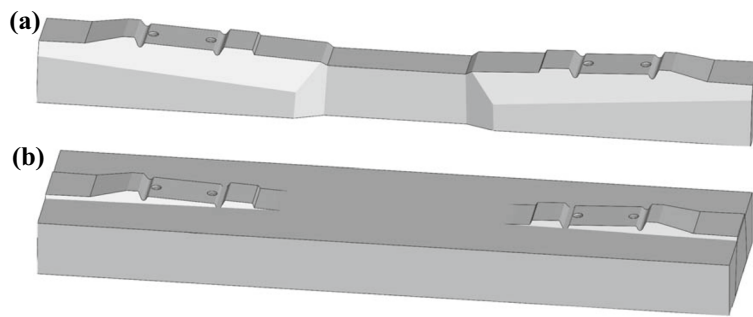


Fig. 3 Relation between the sleeper form and track irregularities



**Fig. 4** The sleeper forms for the simulation: **a** conventional sleeper; **b** wide sleeper

- Particle pressure distribution along the sleeper in zones of maximal impact and vertical loading.

## 2 Methodology

The methodology is based on discrete element modeling of the ballast–sleeper interaction under vertical cyclic loadings. The model aim is to reflect the substantial differences between the wide and conventional sleepers in the settlement accumulation, which are presented by experimental studies (Fig. 2). The settlement accumulation in the experimental studies occurred under 20 million tons of axle loadings, which is practically impossible to reflect in the computationally-intensive DEM simulations. The application of the model in the present study is limited by several thousands of loading cycles. Thus, the complexity of the model is maximally reduced to decrease the calculation time but at the same time to be able to reflect the substantial effects of void accumulation.

Moreover, the chosen particle form is a simple ball that allows the most effective simulation of many loading cycles. The application of simple particle shapes to increase the efficiency of DEM simulations is proposed in other studies [39].

The following assumptions and limitations are noted:

- The sleeper lays on the ballast bed under its own weight; a fully unsupported sleeper hanging on the rails is not introduced.
- The sleeper is an undeformable body with vertical and rotational motion and contact stiffness.
- The ball particles are used with rolling resistance to reflect the particles' angularity.
- The ballast compaction process is not considered. The ballast bed is introduced in maximally compacted form to provide close to linear accumulation of the settlements in the loading cycles.
- Particle breakage and attrition are not considered.
- Maximal sleeper external loading is twice as high as usual to produce reasonable settlement intensities within the acceptable simulation times.

The simulation results, due to introduced assumptions and simplifications, cannot be used for absolute estimation of processes in time. Moreover, the lifecycle time of experimental measurements [1, 4] and the simulation cannot be directly compared. Nevertheless, the results can be used for a relative comparison of conventional and wide sleepers. The maximal possible differences are analyzed at the beginning and the end of the simulation.

The length of the sleeper in the experimental measurements in Fig. 1 [3] is 2.4 m, which is lower than that of the conventional sleeper (2.6 m). Therefore, the sleeper foot forms and lengths for simulations are selected to take into account the differences between wide and conventional sleepers and, at the same time, not to add new factors. The sleeper forms are presented in Fig. 4. The wide sleeper has the same length of 2.6 m as the conventional one but a width of 0.5 m.

The mechanical properties of the sleepers are derived from their geometrical forms and material properties (Table 3). The sleeper form is considered stiff with elastic contact properties: density 2650 kg/m<sup>3</sup>, Young's modulus 20 GPa, and Poisson's ratio 0.3. The degrees of freedom of the sleeper motion are limited to the vertical motion and rotation relative to the track axis.

The applied 3D DEM model considers ball particles that are described by rolling radii, non-linear contact law, tangential stiffness, rolling resistance, etc. The Mindlin–Deresiewicz model is used to describe the tangential force. The Hertzian spring with viscous damping is used as the normal force model. The model scale is 1:1 with a particle size distribution of 22.5–63 mm. The rolling resistance takes into account the influence of the particle form. The values of the model parameters are selected according to experimental and theoretical studies [18, 30, 31, 33, 38, 39]. The ballast layer is filled in a ballast box of a width of 60 cm, and the ballast height under the sleeper is about 30 cm. The sleeper

**Table 3** Mechanical properties of the sleepers

Type	Mass (kg)	Moment of inertia (kg·m <sup>2</sup> )
Conventional sleeper	300	160
Wide sleeper	770	436

sides are filled with particles to provide a ballast bed with 40 cm ballast shoulders and slopes. The ballast bed with sleeper is maximally compacted before simulations. The number of particles depends on the sleeper type: 21,287 particles for a wide sleeper and 25,788 particles for a conventional sleeper. The main material properties of ballast particles and boundaries are listed in Table 4, and the interaction properties of the model between ballast particles, the sleeper and boundaries are presented in Table 5.

The external loading on the sleeper depicts the vertical cyclic loading  $P_c(t)$  on rail seats with a loading cycle of 0.1 s. The sleeper in the DEM simulations is considered as a rigid body, and all external loadings are applied to its mass center. The DEM geometrical model for wide sleepers and the loading diagrams are presented in Fig. 5. Additionally, a loading moment  $M_{ex}(t)$  is applied to depict the eccentric vertical loading and causes the differential vertical settlements. The loading moment is equivalent to 50% of the overload from one rail seat to another  $P_{ex}(t)$ . The period of the moment is 0.2 s, thus the left sleeper side is overloaded in the first vertical cycle, and the right sleeper side is during the second vertical cycle.

The maximal value of the central loading on the whole sleeper is 160 kN and the maximal value of the excentric loading is  $\pm 80$  kN, which is three times higher than the normal one to accelerate the calculations that usually need millions of cycles. The high value is substantiated by time-intensive calculations that are limited by several thousands of cycles. On the other side, the simulation results are considered not absolute but relative to the simulation cases.

The simulation was produced in 3500 loading cycles with saving results each 0.04 s for the long-term analysis. After that, the short-term simulations were produced in the regions of interest to study the dynamic interaction processes with time discretization of 0.001 s.

**Table 4** The main material properties of ballast particles and boundaries

Element	Bulk density (kg/m <sup>3</sup> )	Young's modulus (GPa)	Poisson's ratio
Ballast particles	1700	50	0.3
Ballast box bottom	1600	10	0.3
Right/left ballast box walls	1700	20	0.3

**Table 5** The interaction properties between ballast particles, the sleeper and boundaries

Element	Ballast particle		
	Static friction	Dynamic friction	Restitution coefficient
Sleeper	0.60	0.58	0.72
Ballast particle	0.65	0.61	0.72
Ballast box bottom	0.6	0.58	0.72
Right/left ballast box walls	0.01	0.01	0.65

## 3 Results and analysis

### 3.1 Long-term processes

#### 3.1.1 Sleeper average settlements

After 3500 loading cycles, sleeper center vertical displacements for a conventional sleeper are 78% (or 4.6 times) higher than for the wide sleeper (Fig. 6). In Fig. 6, there are several areas with different sleeper displacement intensities for both sleeper types. Analysis of the change of the inclination angle shows different sleeper behavior for both sleepers (Fig. 7). Initially, the inclination angle for a wide sleeper remains low, stable, and almost unchanged. Approximately in the middle, there is an unstable phase during which significant lateral movements occur at the ends of the wide sleeper. This section will be investigated in detail in the short-term interaction. For a conventional sleeper, there are two long sections (at the beginning of the load and in the middle) with significant inclination angle change, which means multiple lateral movements at the ends of the conventional sleeper.

An analysis of the intensities of sleeper displacements is summarized in Table 6. As expected, the displacement intensity of a conventional sleeper is much higher than that of a wide sleeper. In the unstable phase (in the middle), the sleeper settlement intensity of a conventional sleeper is 62% higher than that of a wide sleeper. Defining features for a conventional sleeper are the most intense lateral movements at the ends of the sleeper from the beginning of cyclic loading. On the contrary, the wide sleeper remains very stable until the unstable phase in the middle. A common property for both sleeper types is the very low displacement intensity at the end of the section, although the intensity of a wide sleeper is 2.3 times lower. The settlements of the conventional sleeper have several unstable zones, while the wide has only one. It could be expected that the wide sleeper could have more unstable zones in the future in the simulations after 3500 cycles.



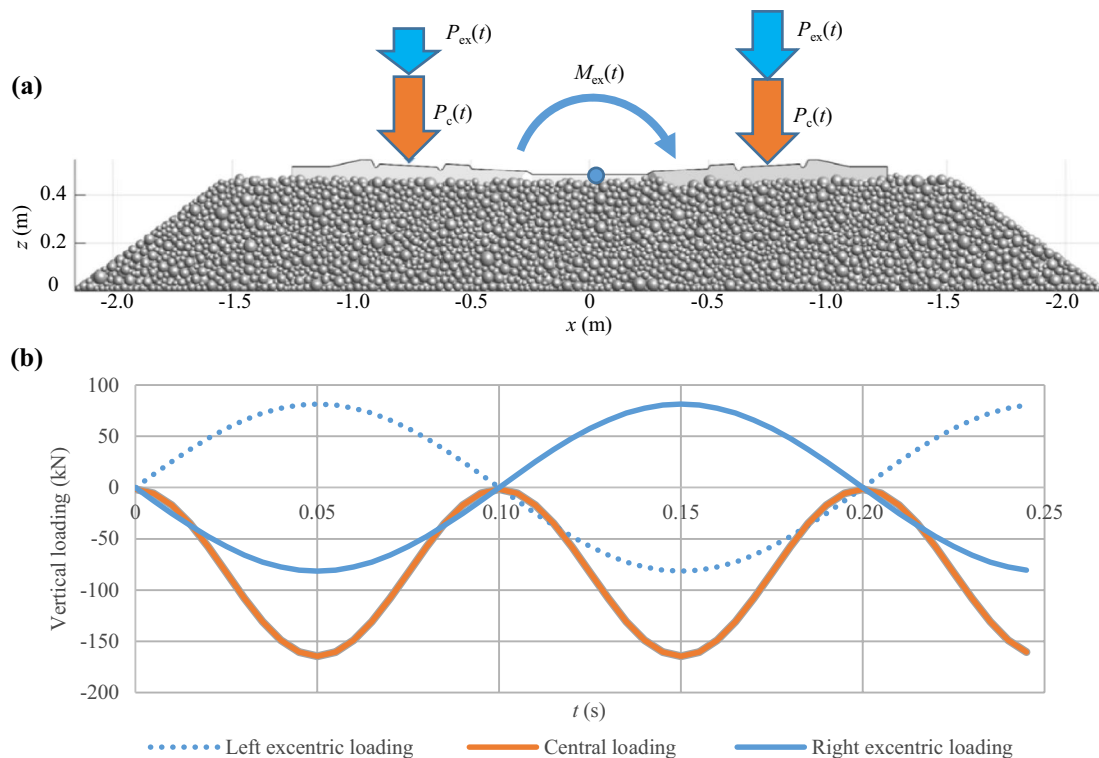


**Fig. 5** **a** Model geometry and **b** sleeper loadings

### 3.1.2 Ballast particle stress evolution

The simulations present a completely different ballast particle stress evolution for both sleeper types (Fig. 8). As we can see, for a conventional sleeper, ballast particle stress distribution changes sharply during all loading cycles. For a wide sleeper, however, the maximal normal force on ballast particles increases enormously only during the period of unstable phase with increased settlement intensity (in the middle time). In comparison with the value for a conventional sleeper, the maximal normal force on ballast particles is 2.6 times lower than for a wide one.

### 3.1.3 Ballast particle flow and ballast layer porosity distribution

Ballast particles move from their initial positions due to numerical loading cycles in accordance with the initial degree of compaction of the ballast layer and, to a great extent, sleeper foot form and particle pressure distribution along the sleeper. Below (Fig. 9), ballast particle flow is depicted after all simulation cycles for two sleeper foot forms. The simulation shows a big difference in ballast particle movement. Under the sleeper foot in the middle part of a wide sleeper, particle movements are almost absent or only minor ones (Fig. 9b). Due to the significant width of a wide

sleeper, ballast particles are limited in their displacement. Their movements start from the ends of a wide sleeper; the particles “try to flow out” of the ballast prism. Near the very ends of a sleeper, the particles protrude upwards. As a result of these displacements, the outline of the ballast prism is getting worse (violated), load processing deteriorates, and stresses and forces in the ballast increase. During the unstable phase, ballast particles move extremely, and the void appears and grows because of an additional uneven load. In the last period, most of the above considered oscillations stabilize in the case of a wide sleeper. Therefore, the flow (movement) of particles also diminishes.

For a conventional sleeper (Fig. 9a), significant displacements are characteristic of almost all ballast particles. Only a negligible number of particles under the sleeper foot in the middle part of a conventional sleeper move slightly. There is a special feature for ballast particles along this sleeper type; therefore, these ballast particles move up in the ballast box and protrude upwards. There are extremely significant displacements at the left and right sides of the ballast prism. The outline of the ballast prism is violated, load transfer is getting worse, and the forces between ballast particles increase. It causes further ballast particle flow, sleeper displacements, and void appearance.

Ballast particle flow is accompanied by intensive mixing of particles, dilation of ballast layer material, and the ballast

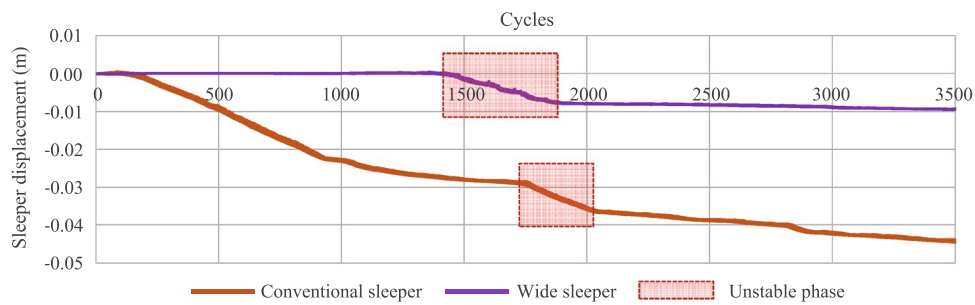


**Fig. 6** Sleeper center vertical settlements

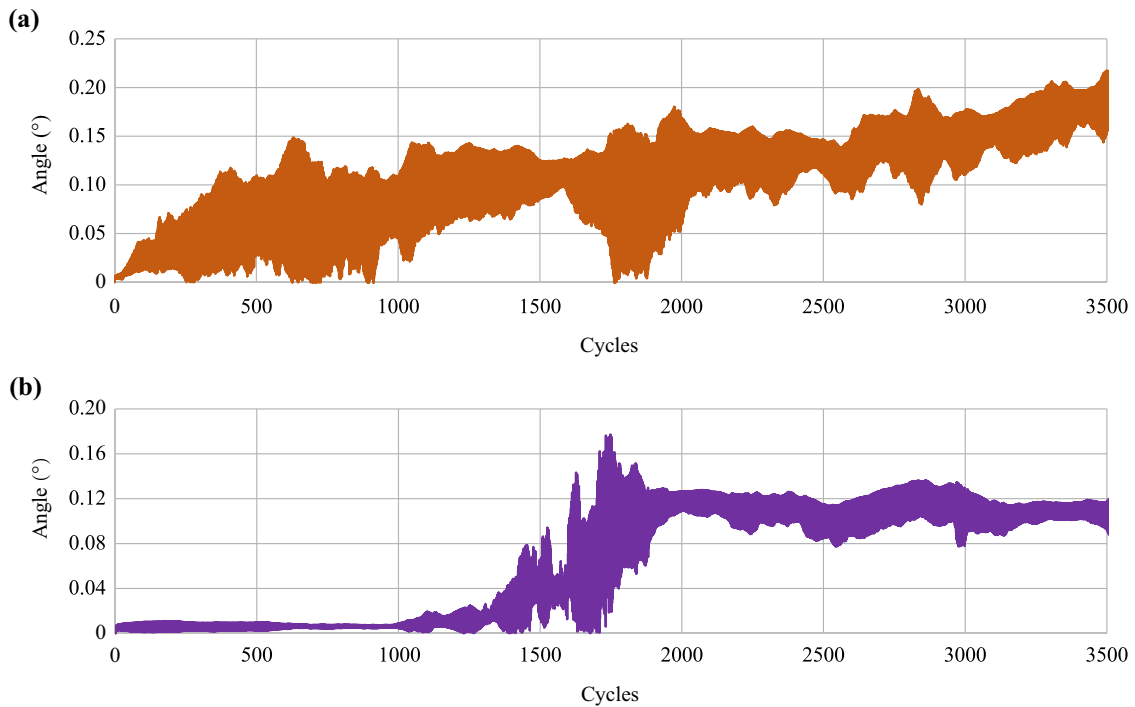


**Fig. 7** Sleeper longitudinal inclination: **a** for a conventional sleeper; **b** for a wide sleeper

uncompacting. The simplest parameter that can present the degree of ballast compaction is the porosity. The estimation of the ballast porosity distribution along the sleeper during the loading cycles for both sleepers is presented in Fig. 10. The porosity is estimated in a zone under the sleeper within the moving square 0.2 m × 0.2 m along the sleeper that

allows acceptable variation and spatial resolution. The ballast layer at the beginning of the cycle loading is maximally compacted, which corresponds to the black lines in Fig. 10. In the starting phase, the average value of the porosity is about 36.3% in the zone under the sleeper for both sleepers. The porosity distribution after whole loading cycles (blue

**Table 6** Intensity of sleeper displacement

Conventional sleeper		Wide sleeper	
Part of the plot	Intensity of sleeper displacement (mm/100 cycles)	Part of the plot	Intensity of sleeper displacement (mm/100 cycles)
At the beginning	-2.8976	At the beginning	-0.0275
In the middle (in unstable phase)	-0.6673	In the middle (in unstable phase)	-1.6468
At the end	-0.3478	At the end	-0.1063

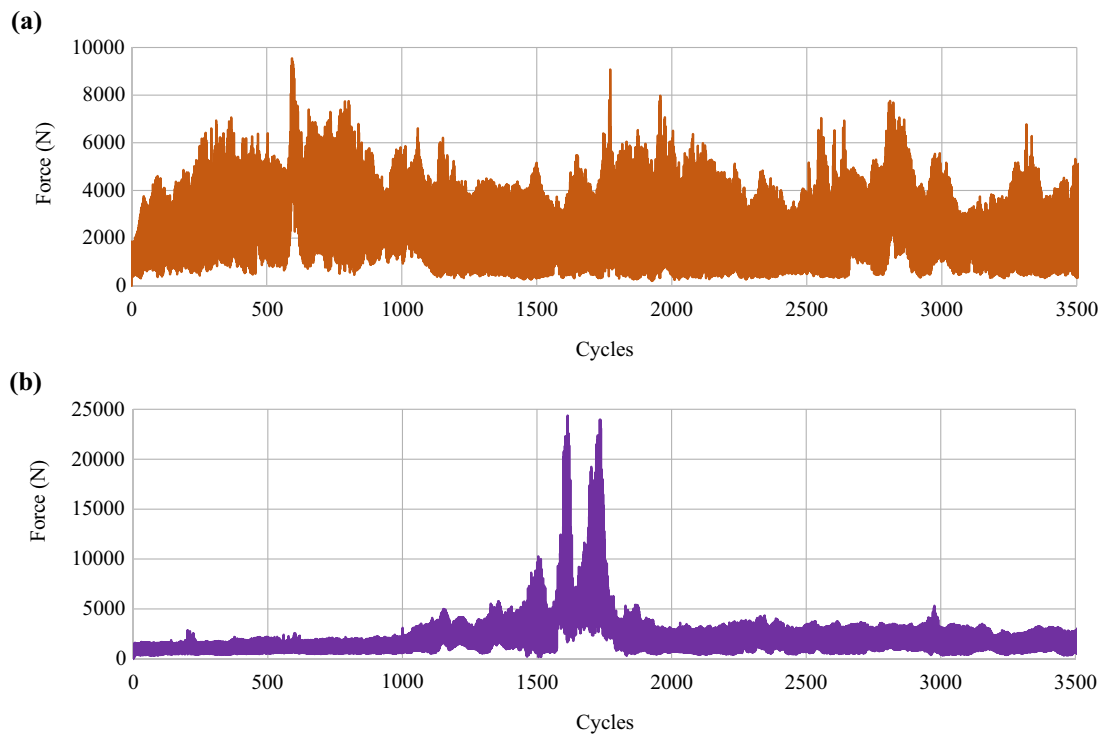


**Fig. 8** Maximal normal force on ballast particles: **a** for a conventional sleeper; **b** for a wide sleeper

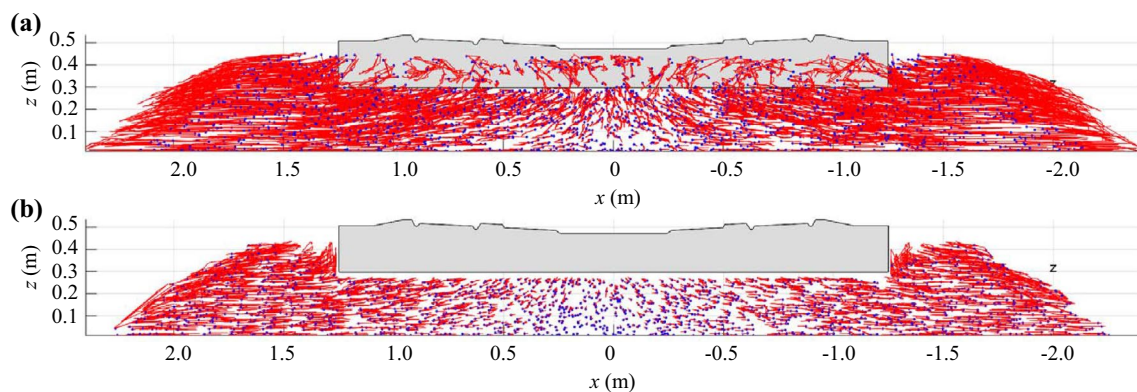


**Fig. 9** Ballast particle flow during whole loading cycles for two sleeper foot forms: **a** conventional sleeper; **b** wide sleeper

line) is noticeably different from the initial state, although the absolute difference is only 2%. The minimal porosity of the fully loosened ballast material is about 38.8%.

The ballast under the ends of the conventional sleeper after the whole loading simulation is almost fully uncompacted. At the same time, the ballast under the central part of the conventional sleeper still has an average porosity of about 37.8%.

The porosity distribution after the loading cycles for the wide sleeper (Fig. 10b) is different from the conventional sleeper case—an about 1% increase of the porosity under

the sleeper ends is obvious in comparison with central part. The absolute porosity of the ballast under the central part of the wide sleeper is about 37%, which, compared to the possible range of porosity variation, is noticeably lower than that of the conventional sleeper. Therefore, the accumulation of the loading cycles results in the overall increase of ballast layer porosity and the especially inhomogeneous porosity distribution under wide sleeper. The temporal development of the porosity appears not gradually in time. The red lines in Fig. 10 present the porosity distribution in the unstable

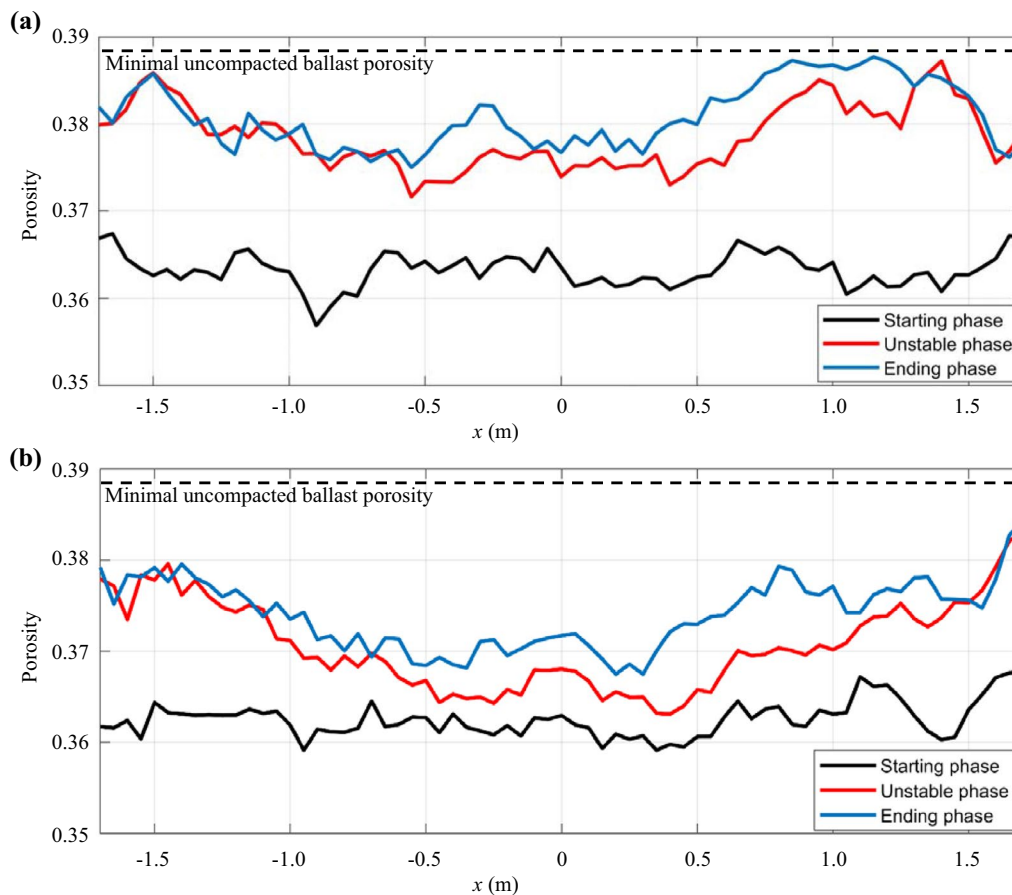


**Fig. 10** Porosity distribution evolution along the ballast box: **a** for a conventional sleeper; **b** for a wide sleeper

zones. Such distribution stays almost the same after the unstable zone with intensive settlements of the sleeper.

### 3.2 Short-time dynamic interaction

In addition, short-term simulations were produced in interest sections: at the beginning of cyclic loading, during the unstable phase, and at the end of cyclic loading. Time discretization is taken in more detail at 0.001 s. Figure 11 depicts how sleeper displacements differ in three periods of time. For a conventional sleeper, vertical center settlements at the beginning achieve 0.23 mm and become five times larger in the unstable phase. During the final load cycles, sleeper center displacements reduce by 30%–35%. For a wide sleeper, the trend for the change in settlements is similar to the conventional one. First, displacements are the lowest, then they increase enormously (7 times higher in the unstable phase), and at the end, they stabilize and become significantly lower. The simulated wide sleeper deflections 0.17–0.23 mm correspond to the track bed modulus 0.635–0.469 N/mm<sup>3</sup>. The derived modulus conforms to the compacted soil and compacted bearing layer: rock, bridge, and tunnel [5]. Therefore,

the track bed stiffness in the model fits the specific cases of the actual engineering conditions. For both sleeper types, significant additional vibration components can be observed in sleeper central displacements during the unstable phase.

Sleeper inclinations during loading cycles were also investigated (Fig. 12). The right and the left ends of the sleepers are loaded one by one. At the beginning of a cyclic loading (Fig. 12a), the inclination angles of both sleeper types are very small. The absolute value of inclination is no more than 0.0085 ° for a conventional sleeper, and 0.0075° for a wide sleeper, although the oscillation pattern and the change of inclination angle during one loading cycle differs for the two sleeper types. At the beginning stage, the wide sleeper inclination changes its values from 0° to 0.0075° but returns to null at the end of each loading cycle. For a conventional sleeper, the angle returns to the values 0.001°–0.0018° at the end of the loading cycle.

During the unstable phase (Fig. 12b), the maximum values of sleeper inclination for a conventional sleeper are 2.3 times higher than for a wide one. The inclination of the conventional sleeper increases abruptly during every cycle from 0.07° to 0.23°, but later the oscillations subside with a

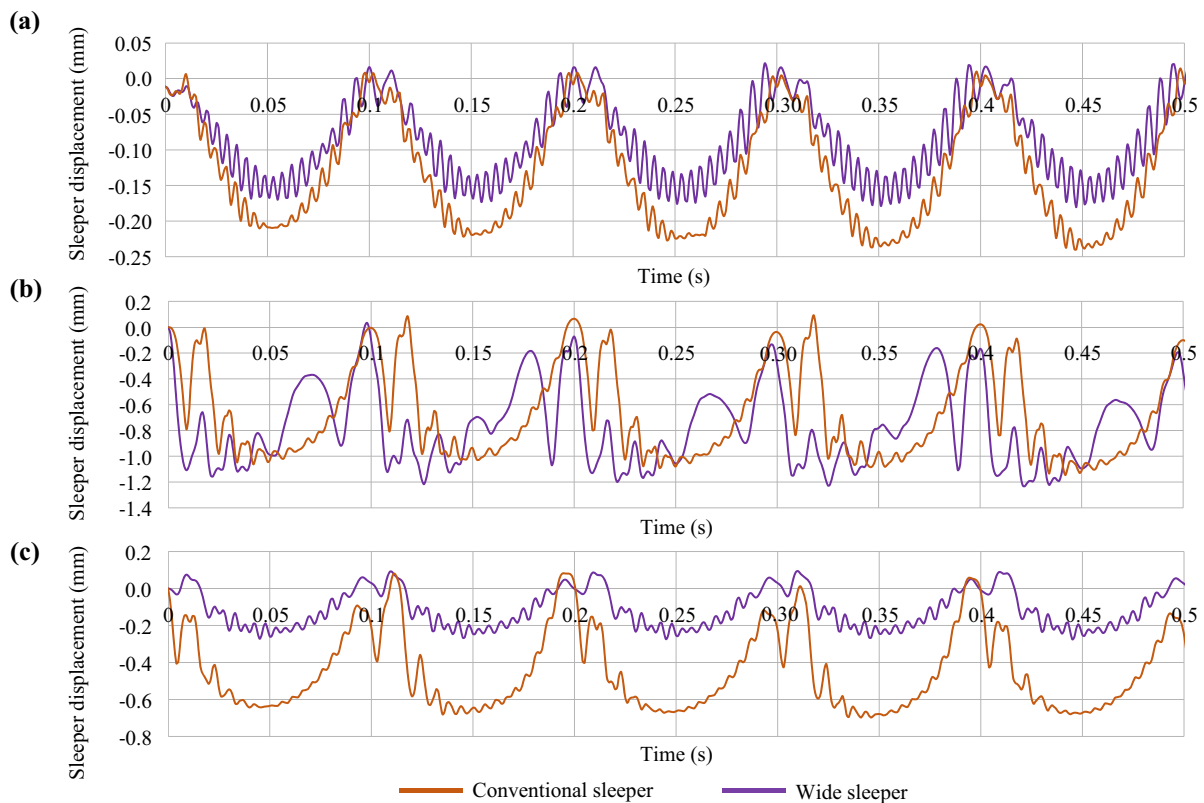


**Fig. 11** Sleeper center displacement during loading cycles: **a** at the beginning of cyclic loading; **b** during the unstable phase; **c** after the unstable phase

negligible amplitude. In this phase, the wide sleeper inclination changes from  $0^\circ$  to  $0.1^\circ$  during every cycle and consists of 5–6 oscillations with significant amplitude.

At the end section (Fig. 12c) for both sleeper types inclination oscillations have a certain initial angle value, below which they do not decrease. The pattern of oscillations looks quite smooth, without sharp jumps within every cycle of the load. Maximum values of sleeper inclination angle are 84% higher for a conventional sleeper than for a wide one.

### 3.2.1 Dynamic interaction in the impact zone

**3.2.1.1 Sleeper's vertical acceleration** The change in the sleeper vertical acceleration during the simulation period is shown in Fig. 13. The vertical acceleration of a conventional sleeper has higher values, especially in the two last phases. For example, in the last section (Fig. 13c), the vertical acceleration of the conventional sleeper is 2.1 times higher than that of the wide one. In the unstable phase (Fig. 13b), this increase is 1.5 times larger. The following change characterizes both sleepers: first, accelerations are relatively low (Fig. 13a), then extremely grow (2.8 and 2.1 times higher for a conventional and a wide sleeper, respectively) (Fig. 13b),

and finally sharply decrease 1.7 and 2.4 times lower, respectively (Fig. 13c). There is a special feature of a wide sleeper: at the end of the simulation period the vertical acceleration of the wide sleep becomes less than at the initial stage.

**3.2.1.2 The ballast particle loading process during the loading cycle** The values of ballast particle loading force (Fig. 14) vary during the simulation period, similar to sleeper center displacements and sleeper inclination. At the beginning (Fig. 14a), ballast particle loading force acquires almost the same values for both sleeper types or up to 25% more in the case of a conventional sleeper.

This force increases extremely in the period of unstable phase: for a conventional sleeper up to 3.7 times higher, and for a wide sleeper—up to 5.8 times higher (Fig. 14b). Very unexpectedly, the ballast particle loading force on this section for a wide sleeper exceeded this force for a conventional one by 1.4 times. Such excess values of a wide sleeper are not typical.

In the last section (Fig. 14c), the representation of the ballast particle loading force is similar to the one at the beginning but with larger values. Thus, for a wide sleeper, twice higher force values are presented, and for a conventional sleeper, approximately 2.6 times higher. In the end,

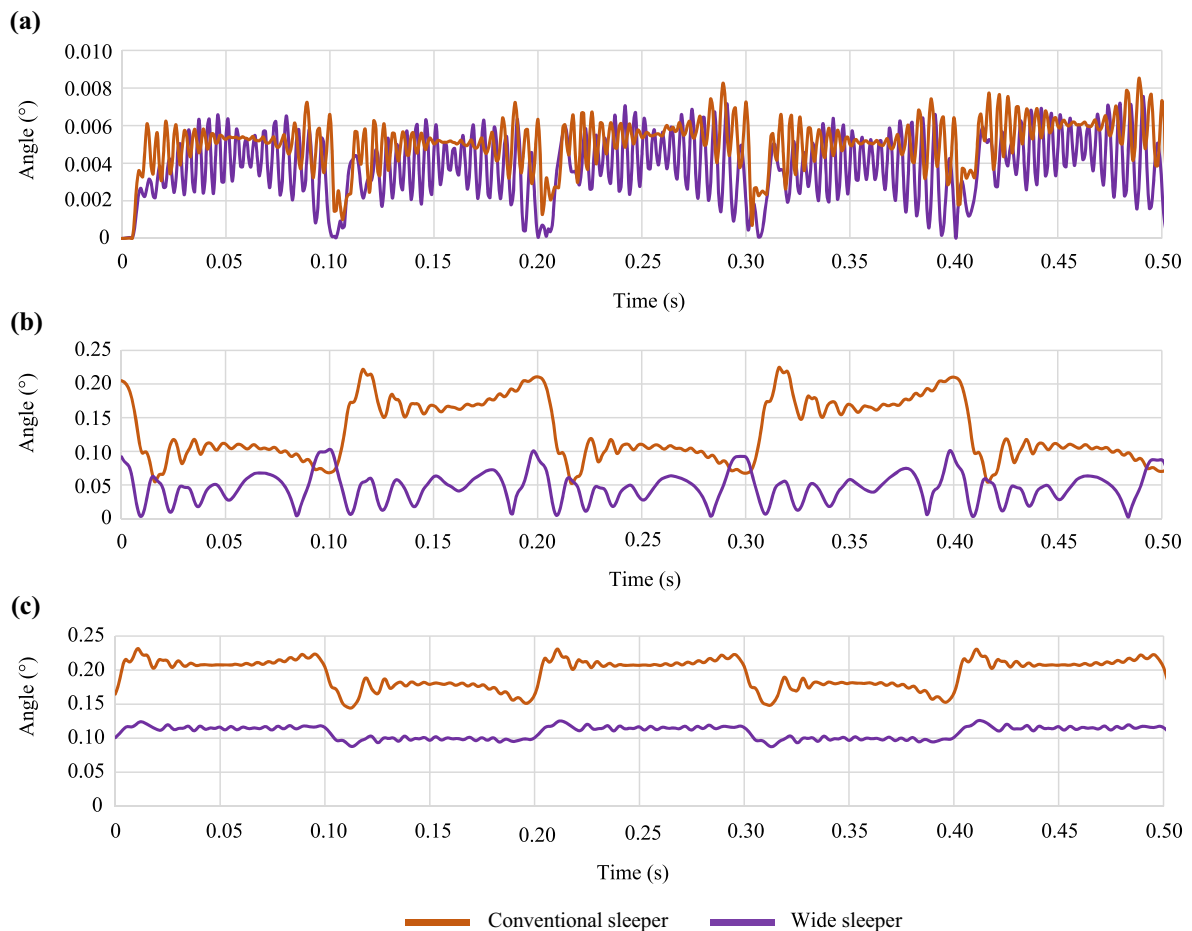


**Fig. 12** Sleeper inclination during loading cycles: **a** at the beginning of cyclic loading; **b** during the unstable phase; **c** after the unstable phase

the ballast particle loading force for a conventional sleeper is higher again than for a wide one (up to 46%).

**3.2.1.3 Particle surface form under the sleeper foot and geometrical void distribution along the sleeper** During the simulation, particle pressure distribution along the sleeper, particle surface form under the sleeper foot, and geometrical void distribution along the sleeper were calculated and compared for both sleeper types.

The distribution of void and ballast particle loading in the moment of maximal quasistatic loading is presented in Fig. 15. In Fig. 15b, the cross-section of a ballast bed with a ballast bed with a wide sleeper is depicted with ballast particles, which perceive and redistribute the load. As can be seen, during the unstable phase, a low number of ballast particles is involved in load transfer. The proportions of a ballast prism are damaged as a result of incorrect interaction of railway track elements due to the appearance of a void under the sleeper foot (Fig. 15a). As can be observed, on the left end of a wide sleeper, an unsupported zone appeared.

Particle pressure distribution along the sleeper is displayed below (Fig. 15c). On the right side of the sleeper, which is under the load, there are sharp peaks of the mean normal force (red line) and concentration of significant values of the maximal normal force for separate particles (blue points).

**3.2.1.4 Particle pressure distribution along the sleeper** Particle pressure distribution along the sleeper during the three time phases, for a conventional sleeper is shown in Fig. 16 and for a wide one in Fig. 17. The mean normal force during the initial load period is almost similar for the two sleeper types both in form and in numerical values (Fig. 16a and Fig. 17a).

During the unstable phase, the mean normal force increases 1.9 times in the case of a conventional sleeper (Fig. 16b). We can see that the length of pressure distribution decreases by approximately 0.5 m at the unloaded sleeper end, and load transfer deteriorates circa 0.4 m at another sleeper end with applying a load. Peaks in value

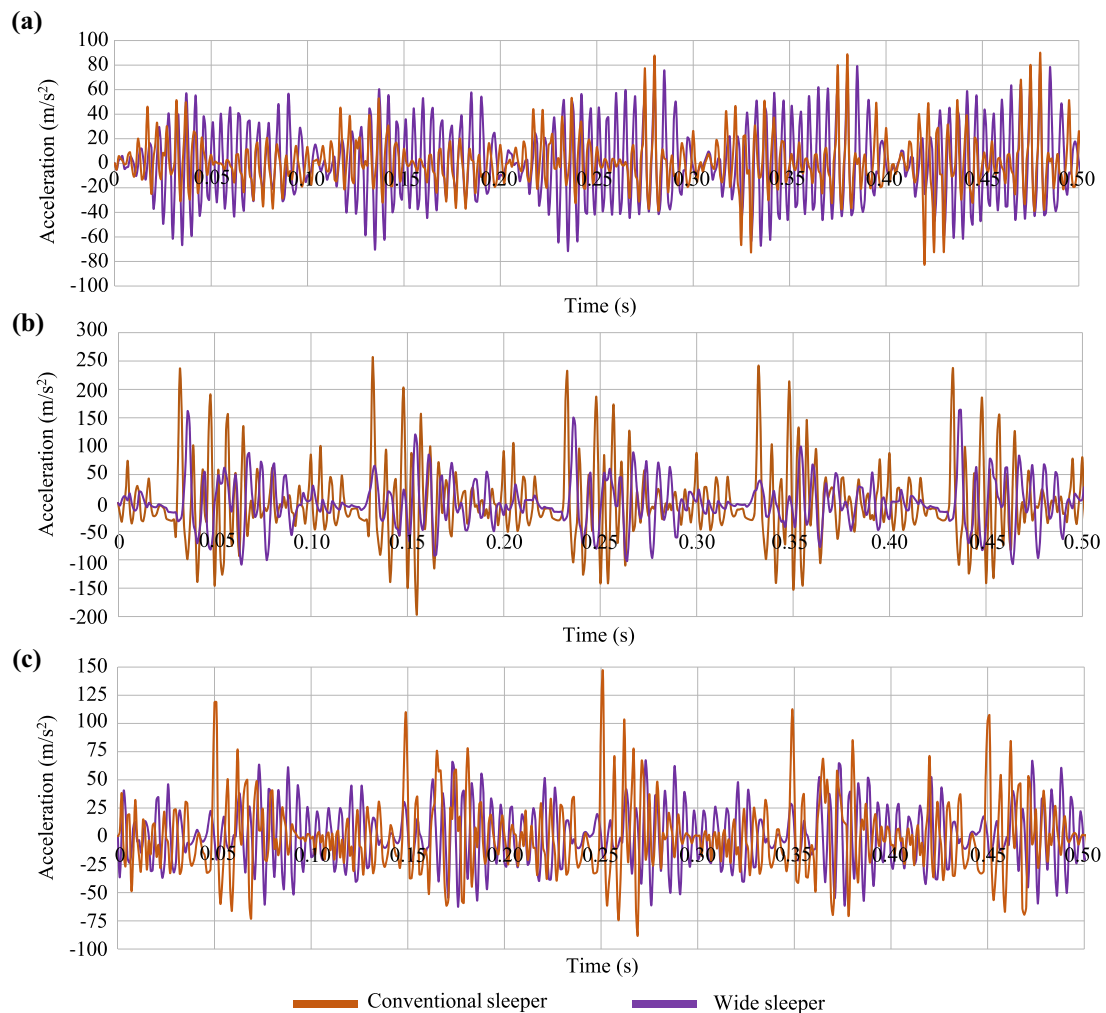


**Fig. 13** Sleeper's vertical acceleration during loading cycles: **a** at the beginning of cyclic loading; **b** during the unstable phase; **c** after the unstable phase

changes become noticeable, and particle pressure distribution becomes uneven.

In the last phase (Fig. 16c), the mean normal force values are higher than those at the beginning. As can be seen, the area with ballast particles that perceive the predominant load is shifted to the middle of a conventional sleeper, compared to the initial stage.

For a wide sleeper, the mean normal force increases 2.2 times in the unstable phase (Fig. 17b). Similar to a conventional sleeper, the length of pressure distribution along the sleeper decreases. But this reduction is longer for a wide sleeper and is equal to 0.8–0.9 m at the sleeper end without applying a load and 0.5 m at a loaded sleeper end. Peaks are even sharper than for a conventional sleeper and contain up to a third of the mean normal force in general.

In the last phase (Fig. 17c) the mean normal force increases slightly compared to the initial time (only up to 10%) because, at the end of the observation time, the ballast

under the wide sleeper stabilizes under the load. The trend line of the particle pressure distribution differs from the initial one with sharper peaks and the decrease in length of pressure distribution along the sleeper.

**3.2.1.5 Particle loading comparison during maximal impact loading and maximal overall loading** A detailed analysis of zones of maximal impact during one loading half-cycle in the unstable phase for a conventional sleeper (Fig. 18) was performed. The ballast particle maximal loading (Fig. 18a) consists of overlapping dynamic and quasistatic parts. The dynamic part occurs due to closing the void under the sleepers, and the quasistatic one is due to external loading on the sleeper. The corresponding sleeper's vertical acceleration (Fig. 18b) shows two groups of oscillations: at the beginning of the cycle with the maximum peak at the moment 0.332 s and in the middle time 0.345–0.365 s before the maximal quasistatic loading. The sleeper acceleration in the time of

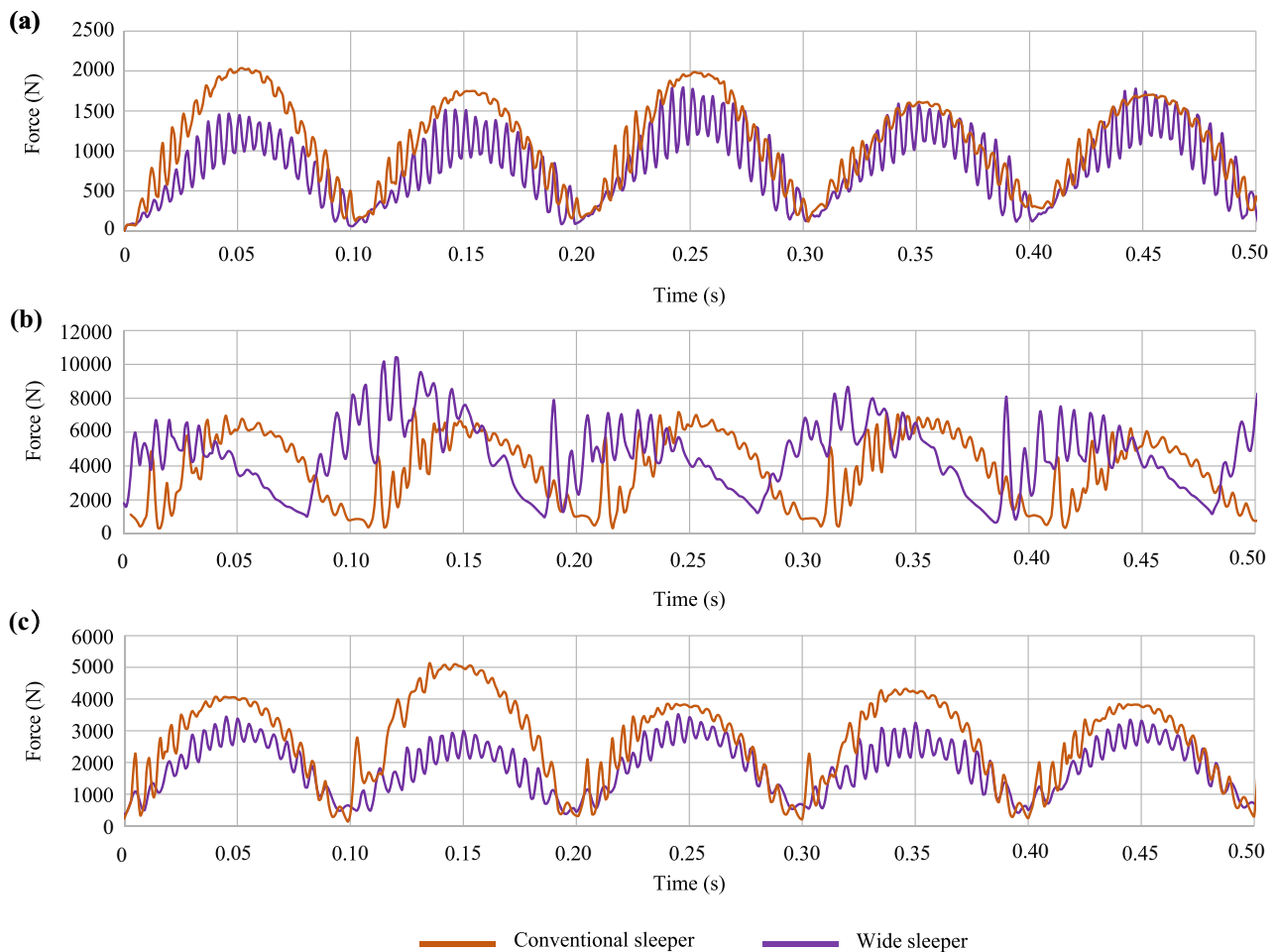


**Fig. 14** Ballast particle loading force during loading cycles: **a** at the beginning of cyclic loading; **b** during the unstable phase; **c** after the unstable phase

maximal quasistatic loading is many times lower than that in the impact time, while the particle's overall maximal loadings are comparably close.

The particle loading distribution along the sleeper (Fig. 18c) in the times of the loading maximal peaks shows the differences in loading transmission over the ballast layer. Clear two groups of loading distribution are visible: one group under the central-right part of the sleeper and another group of 2 lines at the sleeper end (0.339–0.344 s). The maximal quasistatic loading time of 0.376 s corresponds to the maximal particle loading under the central part of the sleeper in the zone with the  $x$ -coordinate from  $-0.5$  to  $0.9$  m. However, the loading distributions for some impact moments (0.332 s, 0.348 s) are similar to the quasistatic loading under the central part of the sleeper. Thus, the loading distribution during the first impact at 0.332 s with low quasistatic loading demonstrates low particle loading under the sleeper end except the loading under the right side of the sleeper. This phenomenon, as well as two groups of oscillations in the diagram of the sleeper accelerations, can be

explained with the sequential void closing under the central-right part of the sleeper and the following void closing under the sleeper end.

## 4 Discussion

The previous experimental studies on the application of wide sleepers on the ballast layer have shown that they are very effective for the reduction of longitudinal track irregularities. However, the development of cross-level track irregularities for wide sleepers is as high as in the track with the conventional sleepers. Studying the explanation of the reason was the initial motivation for the present research. DEM simulations were carried out to study the cross-level irregularities accumulation for both wide and conventional sleepers. A simple model with one sleeper under the vertical eccentric cyclic loading and simple ball particles was applied. The model, due to many assumptions, like a stiff sleeper,



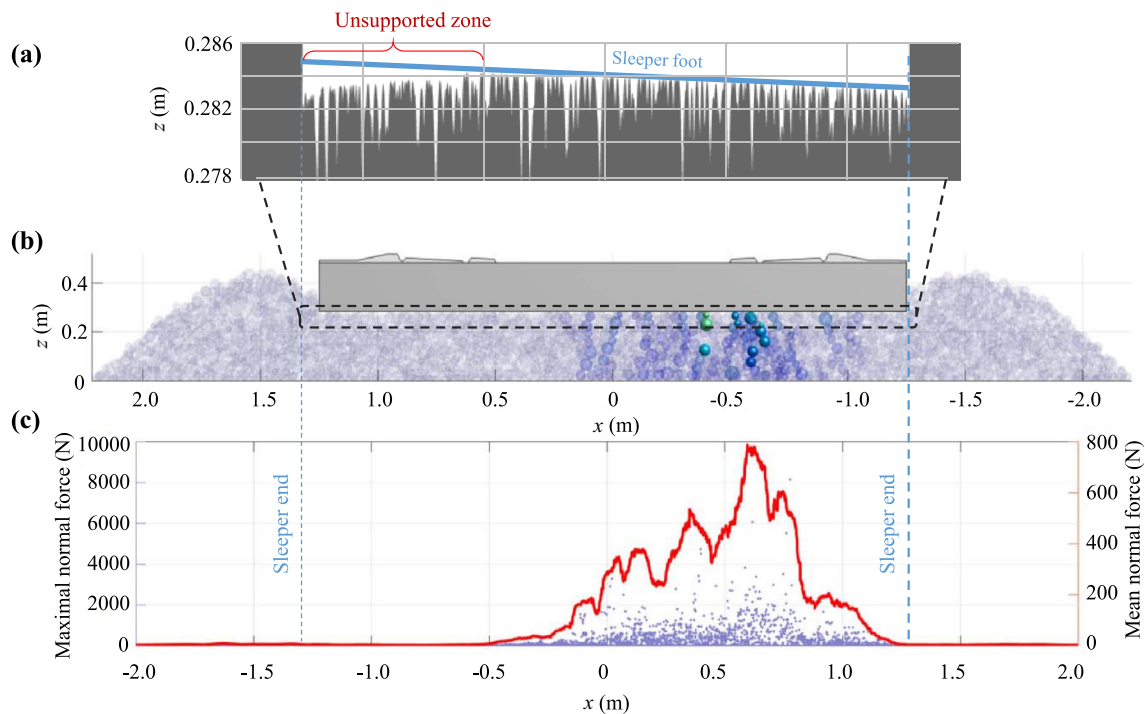


**Fig. 15** **a** Distribution of the void under the sleeper foot; **b** a cross-section of load transfer in the ballast bed; **c** ballast loading distribution along the sleeper

over-dimensional loading, no full contact, etc., is far from reality and does not allow direct absolute comparison with the experimental results. However, the model is complex enough to reflect the main intrinsic processes of interaction in the void zone: impact, loading concentration in the central part of the sleeper, ballast flow, and settlements. Therefore, the simulation results are considered not absolutely but relatively between wide and conventional sleepers. Further discussion is focused on the analysis of sleeper differential settlements that cause track geometry failures. Moreover, the internal short-term and long-term processes in the ballast layer are analyzed to study the mechanism of the settlement accumulation.

#### 4.1 Analysis of sleeper differential settlements

The most important comparison parameters of track geometry deterioration are sleeper average and differential settlements, as well as their intensities. The comparison of the sleeper average displacements (Fig. 6) shows quite different processes for the wide and conventional sleepers. The conventional sleeper starts the intensive accumulation of residual settlements after a short time (150 cycles), while the wide sleeper keeps the stable position for up to 1400 loading cycles. The process of settlement accumulation after the stable zone is complex: one or many

unstable zones with high settlement intensity appear. The wide sleeper has one unstable zone in the middle part of the loading cycle with very high intensity. After that, the following settlement accumulation rate is constant and low. The conventional wide sleeper shows three unstable zones with a high settlement rate, but each next one is lower than the previous one. It is not possible to say when the unstable zone is and how many of them could appear during the real lifetime of the ballast bed. Therefore, the maximal possible values are compared to the overall simulation time. The comparison of the settlements (Table 1) shows that the maximal settlement intensity is up to 3.5 times lower for the wide sleeper, and its overall settlement is up to 4 times lower than that of the conventional sleeper. The approximate comparison with the experimental data (Table 2) is possible in the parameter “longitudinal level” that shows a 2.75 times lower value for wide sleepers than for conventional sleepers. However, the experimental measurements, different from the simulation results, do not take into account the homogenous settlement of the ballast bed.

The other important parameter of the interaction is the differential settlements that are here expressed is sleeper inclination (Fig. 7). The maximal variation of the sleeper inclination corresponds to the unstable zones in the settlement intensity process (Fig. 6). The absolute value of the sleeper inclination corresponds to the cross-level

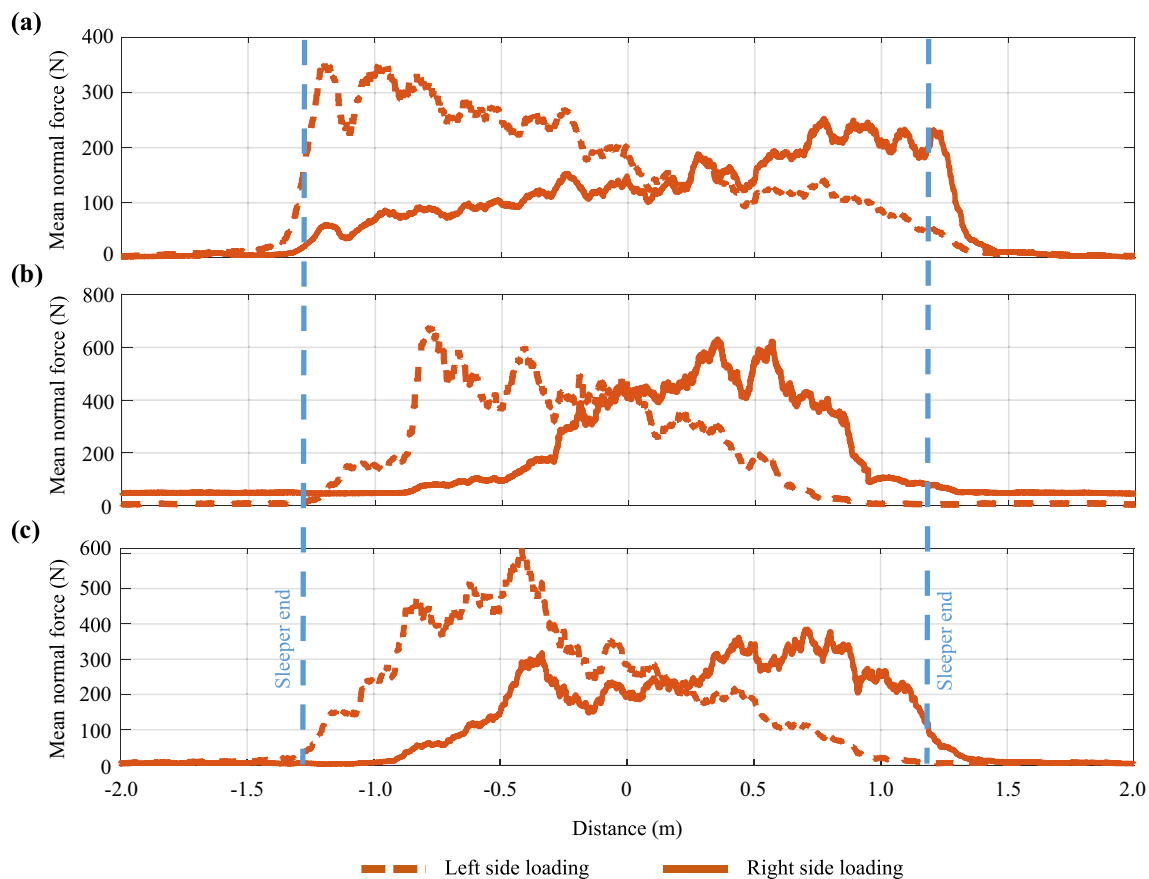


**Fig. 16** Particle loading distribution along the conventional sleeper in zones of maximal vertical loading during loading cycles: **a** at the beginning of cyclic loading; **b** during the unstable phase; **c** after the unstable phase

irregularity and the differential inclination to the void variation along the sleeper. The absolute inclination of a wide sleeper at the end of the loading cycle is about 1.7 times lower than that of a conventional one. However, the value during the unstable zone is almost the same for both sleepers. The maximal reached differential inclinations of the sleepers are almost the same:  $0.15^\circ$  for a conventional sleeper and  $0.16^\circ$  for a wide one. It corresponds to a 3.5 mm void opening under the sleeper end. The voids after the unstable zones are smoothed and stay about constant within  $0.02^\circ$ – $0.05^\circ$  for both sleepers. The simulated sleeper inclinations agree with the experimental measurements (Table 2) of the cross-level and twist irregularities, indicating almost the same or even worse track geometry quality for wide sleepers than for conventional ones. It should be noted that the wide sleeper in the experimental investigations is 0.2 m shorter than the conventional one, which could cause additional cross-level differential settlements.

#### 4.2 Mechanism of the cross-level differential settlements accumulation

The simulated geometrical parameters of the wide sleeper behavior in a cross-level show similar behavior as in experimental studies. However, they cannot explain the reasons for the behavior and the mechanism of its development. Thus, the additional parameters of the long-term processes are analyzed like ballast particle loading in relation to the ballast settlements, distribution of the particle loadings along the sleeper, particle flow, ballast porosity, as well as the short-time interaction: sleeper motion, acceleration, and forces during the loading cycle.

The first indication of the reason for the intensive settlements and unstable zones is the accumulation of the differential inclination that precedes the start moment of intensive settlement accumulation in the unstable zone. The intensive accumulation of voids for a wide sleeper (Fig. 7) started long before the start of the intensive vertical settlements (Fig. 6).

Another indicator of intensive ballast deformations is the maximal particle loading (Fig. 8), where the times of the peaks of the loadings correspond to the time of the unstable

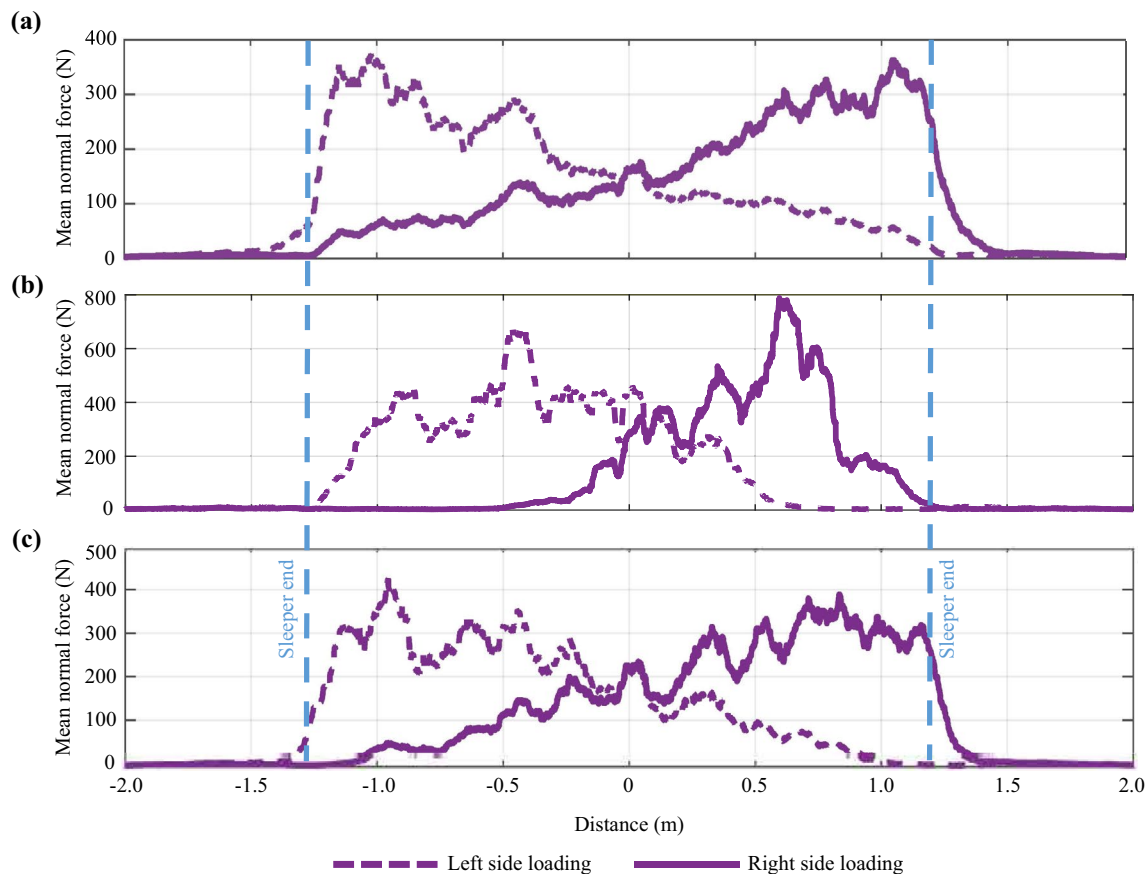


**Fig. 17** Particle pressure distribution along the wide sleeper in zones of maximal vertical loading: **a** at the beginning of cyclic loading; **b** during the unstable phase; **c** after the unstable phase

zones. The peaks are especially distinctive for a wide sleeper (Fig. 8b) with ten times higher maximal values than for the stable zones. Moreover, the maximal particle loading for a wide sleeper is up to 2.5 times higher than for a conventional one. Such extremal particle loadings indicate either some concentration of the sleeper loading or on small ballast area or impact of the sleeper.

The comparison of the maximal ballast particle loading process during the loading cycles (Fig. 14) shows more than two times increments of the quasistatic particle loadings from the initial time moment to the end of the cycles. Additionally, the impact interaction is visible in the starting moment of loading cycles or the sleeper inclination moment. The impact of the sleeper foot on the ballast bed occurs due to void closing. Thereby, the particle loading in the impact moment reaches up to 50% of the quasistatically caused particle loading. The impact interaction is also clearly visible on the short-time diagrams of sleeper displacements (Fig. 11), sleeper inclination (Fig. 12), and sleeper vertical acceleration.

The spatial distribution of the particle loadings under the sleeper during the loading cycle is examined to find out the

reason for the loading concentration. A visualization of the sleeper foot and ballast bed interaction in the moment of the maximal external loading (Fig. 15) demonstrates the concentration of loading transition on the ballast layer within the small area of the ballast bed between 0 and 0.8 m of the sleeper length. Therefore, the maximal particle loading is more than three times higher than that of good sleeper support in the first loading cycles. The left 0.8 m side of the sleeper foot is lifted with a maximal 3 mm void beneath. Comparison of particle loading distribution for conventional (Fig. 16) and wide sleeper (Fig. 17) before, during, and after the loading cycles show how well the external loading transmitted over the ballast layer. The diagrams of the mean normal force in the beginning cycles (Fig. 16a and Fig. 17a) are close to the triangular form with the maximal value near the sleeper ends. The loading is transmitted over the whole area of the ballast under the sleeper. On the other hand, the particle loading distribution after whole loading cycles (Fig. 16c and Fig. 17c) is concentrated on a smaller area, about 80% of the sleeper length, with up to 30 cm fully unloaded zones under sleeper ends. The loading distribution zone in the time of intensive settlements (unstable zone) is

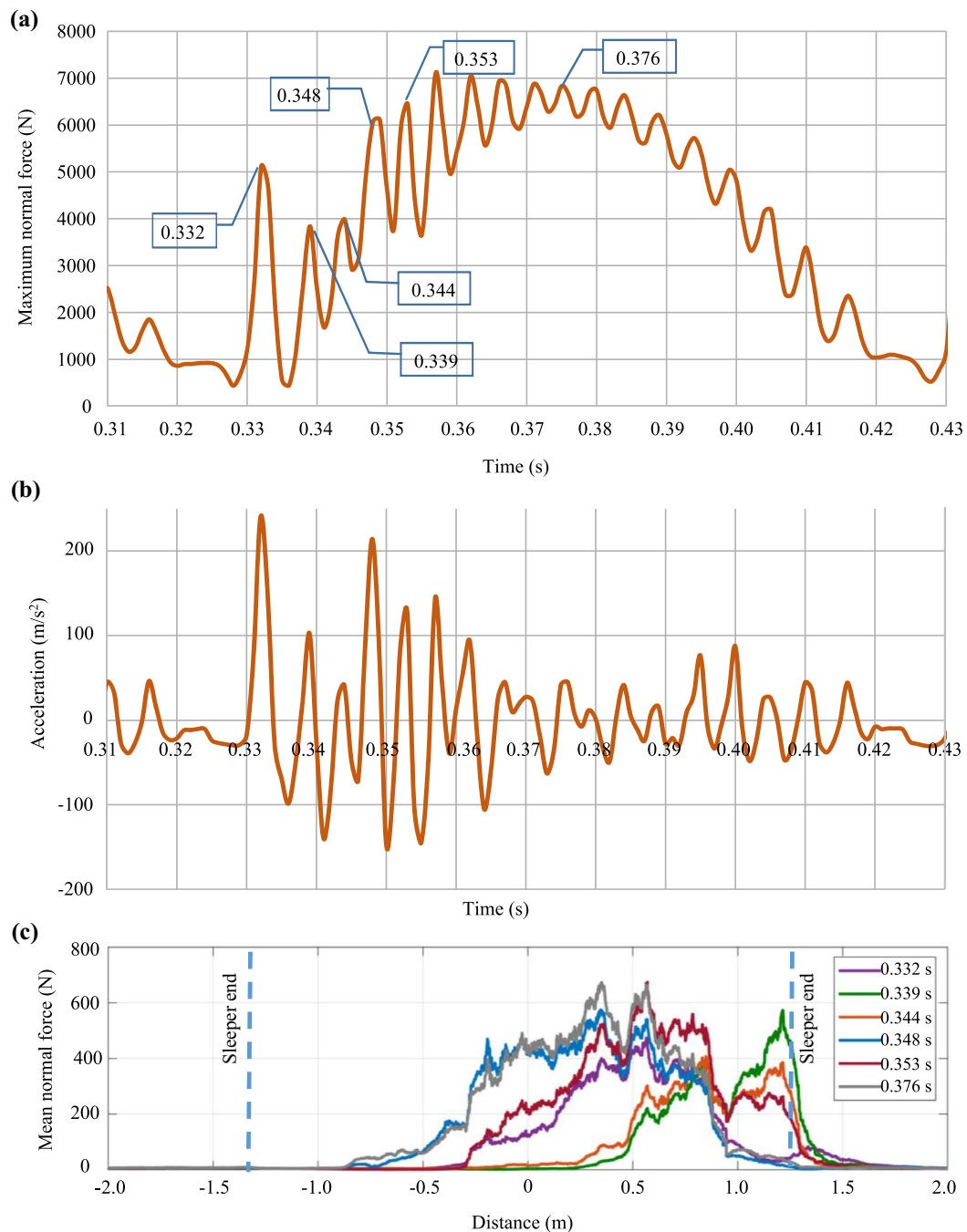


**Fig. 18** **a** The time history of the maximal particle-sleeper loading, **b** sleeper acceleration, and **c** ballast particle mean loading distribution along the sleeper during one cycle of impact loading

even smaller. Only up to 60% of the ballast area under the sleeper is loaded for a conventional sleeper and up to 50% for a wide sleeper. It results in higher maximal loading of the particles.

The detailed analysis of the process of sleeper-ballast impact (Fig. 18) shows that the impact process consists of a series of impacts with various amplitudes and zones of loading transmission. The highest dynamic loading occurs

during the first impact in time with low quasistatic loading. The following lower impacts are superposed with the quasistatic loading and can have higher overall loading. Notable is the small zone of ballast loaded in time during the impacts between the first impact and the maximal quasistatic loading. The zone is 30%–40% of the whole length of the sleeper and corresponds to the void zone. Therefore, the void zones are loaded with impact and concentrated loadings.

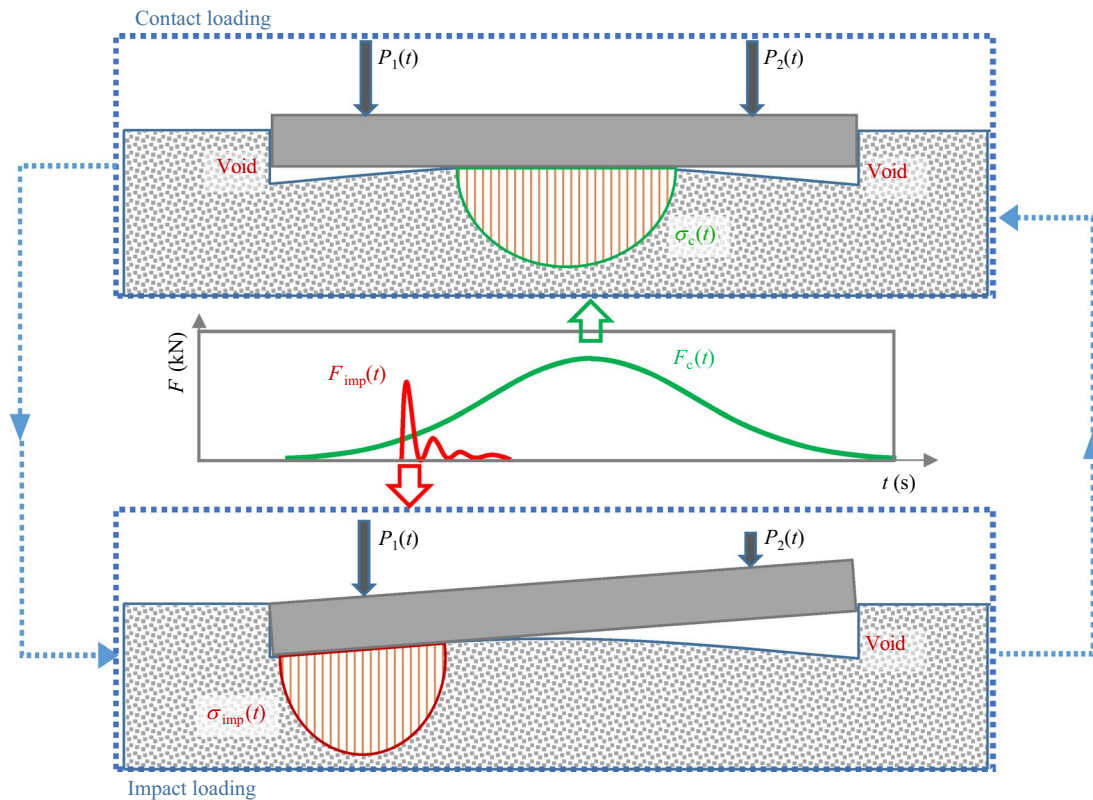


**Fig. 19** Supposed mechanism of void development along the sleeper. Here,  $P_1(t)$  and  $P_2(t)$  are quasistatic loading on the left and right rail support, respectively;  $F$  is load on the ballast in kN, and  $t$  is time in s;  $F_c(t)$  is quasistatic loading and  $F_{imp}(t)$  is impact loading on the ballast layer;  $\sigma_c(t)$  is contact pressure on the ballast;  $\sigma_{imp}(t)$  is impact ballast pressure under the sleeper end

The diagrams of ballast particle flow (Fig. 9) explain the reasons for the appearance of the loading concentration zones. The ballast particle flow for the conventional sleeper is more homogeneously distributed than for the wide sleeper, and the particles flow in the zone between the sleepers. At the same time, the particles under the sleeper central part of the wide sleeper are almost not subjected to flow. Therefore, the ballast is confined in the central zone that has low settlement intensity compared to the side zones that facilitate the development of voids.

Ballast particle flow causes particle mixing, dilation of ballast layer material, and the reduction of porosity. The ballast porosity distribution (Fig. 10) is different for wide and conventional sleepers. The porosity after the cyclic loading is inhomogeneous along the sleeper, especially in the case of the wide sleeper. Consequently, more porous material causes higher vertical settlement intensities. The lower porosity under the central part of the wide sleeper is the result of lower particle flow there (Fig. 9), which causes different settlement intensities and cross-level irregularities.

Based on the presented analysis, the simplified mechanism of the short-term dynamic interaction and the long-term differential settlements can be concluded (Fig. 4). The mechanism consists of two processes: ballast dynamic

impact in sleeper ends and pressure concentration at the sleeper center. The voids under the sleeper end induce impact and vibration that cause the differential ballast settlement along the sleeper (Fig. 19, bottom). On the other side, the differential settlements cause a redistribution of the quasistatic loading and its concentration to the sleeper center and, thus, more intensive settlements in the central part of the sleeper. If the second factor overcomes the first, the voids will be smoothed by the sleeper foot.

The interaction from Fig. 19 suggests the appearance of an equilibrium state where both the factors mentioned above are compensated, and the void form along the sleeper is constant. However, the simulations show the existence of sequences of unstable zones where one factor is dominant. The effect could be explained by the influence of the granular material, its compaction, and uncompacting during flow.

The practical value of the research consists of hints to the design of the sleeper foot. The increase in the sleeper width would likely improve its resilience to settlement development. However, the increase of the sleeper foot in its central part is contra-productive for the resilience to cross-level irregularities—the confined ballast in the central part facilitates the growth of the differential settlements in cross-level. The conventional sleeper design with a narrow central part

allows better the ballast particle flow in the zones between the sleepers, and its confined zone is much smaller than that of wide sleepers. However, the particle flow under the sleeper ends is quicker than in the central part, which causes differential settlements along the sleeper.

The sleeper support at many points cannot be stable and will always cause some voids. The ideal void-free sleeper design would suppose two-point support of sleepers or equal ballast flow under the sleeper and outside it. The ladder sleeper [2] or twin sleeper designs with almost absent central support would probably further improve the performance to cross-level resilience.

## 5 Conclusions

The following main conclusions could be formulated from the study:

- 1) The effect of “sleeper riding”, its mechanism, and its relation to the sleeper form have been studied in the paper.
- 2) Wide sleepers/slabs on the ballast layer have up to 3.5 times lower intensity of the vertical settlements than the conventional mono-block sleepers but similar differential settlements at cross-level.
- 3) The reason for the behavior is the low settlement intensity of the confined ballast under the central part of the wide sleeper. The ballast central part under the conventional sleeper is less confined due to the particle flow between the sleepers.
- 4) The ballast layer under the sleeper ends is subjected to intensive settlements due to sleeper-ballast impacts while void closing.
- 5) The zone of active loading transmission from the sleeper to the ballast after the appearance of the void along the sleeper is reduced up to the half sleeper length, which correspondingly increases the ballast loading.
- 6) Sleeper voids and inhomogeneous support along the sleeper cause intensive sleeper cross-level settlements.

**Acknowledgements** The authors would like to acknowledge Rhomb-erg Sersa Deutschland Holding GmbH for their data and financial support. Also the authors would like to acknowledge the support from the Philipp Schwartz-Initiative of the Alexander von Humboldt Foundation.

**Open Access** This article is licensed under a Creative Commons Attribution 4.0 International License, which permits use, sharing, adaptation, distribution and reproduction in any medium or format, as long as you give appropriate credit to the original author(s) and the source, provide a link to the Creative Commons license, and indicate if changes were made. The images or other third party material in this article are included in the article’s Creative Commons license, unless indicated otherwise in a credit line to the material. If material is not included in

the article’s Creative Commons license and your intended use is not permitted by statutory regulation or exceeds the permitted use, you will need to obtain permission directly from the copyright holder. To view a copy of this license, visit <http://creativecommons.org/licenses/by/4.0/>.

## References

1. Unbehaun O (2000) Breitschwelengeleises—erste testergebnisse. *Eisenbahningenieur* 51:106–113 (in German)
2. Wakui H (1998) Technological innovation in railway structure system with ladder sleeper. *Concr J* 36(5):8–16
3. Deutsche Bahn AG (2014) *Betonschwellen feste fahrbahn fertigteiltragplatten komponenten im netz der deutschen bahn AG*, 1st edn. Betonschwellenindustrie e.V, Berlin
4. RAILONE (2023) Breitschwelle: so breit, so gut! <https://www.railone.de/produkte-loesungen/fern-gueterverkehr/schotterob-erbau/sonderoberbau/breitschwelle>. Accessed 24 Feb 2023
5. Lichtberger B (2005) *Track compendium: formation, permanent way, maintenance, economics*. Eurailpress, Hamburg
6. Shannon Rail Services (2002) Twist faults. [Guidelines]. [https://shannonrail.com/wp-content/uploads/pwi/twist\\_faults.pdf](https://shannonrail.com/wp-content/uploads/pwi/twist_faults.pdf). Accessed 24 Feb 2023
7. Bergquist B, Söderholm P (2015) Data analysis for condition-based railway infrastructure maintenance. *Qual Reliab Eng Int* 31(5):773–781
8. Stibler M (2014) *Der Oberbau der GKB am Prüfstand*. Dissertation, TU Graz. <https://diglib.tugraz.at/download.php?id=576a7303ee64d&location=browse>
9. Feurig S (2020) *Experimentelle und theoretische Untersuchungen zur Optimierung des Dynamischen Gleisstabilisators (DGS) im Hinblick auf eine Verbesserung der Gleislagestabilität*. Dissertation, TU München. <https://mediatum.ub.tum.de/doc/1544877/document.pdf>
10. Lundqvist A, Dahlberg T (2005) Load impact on railway track due to unsupported sleepers. *Proc Inst Mech Eng Part F J Rail Rapid Transit* 219(2):67–77
11. Holtzendorff K (2003) *Investigation of the settlement behavior of railway ballast and the void forming on railway tracks*. Dissertation, Technische Universität Berlin
12. Zhu JY, Thompson DJ, Jones CJC (2011) On the effect of unsupported sleepers on the dynamic behavior of a railway track. *Veh Syst Dyn* 49(9):1389–1408
13. Bezin Y, Iwnicki SD, Cavalletti M et al (2009) An investigation of sleeper voids using a flexible track model integrated with railway multi-body dynamics. *Proc Inst Mech Eng Part F J Rail Rapid Transit* 223(6):597–607
14. Recuero AM, Escalona JL, Shabana AA (2011) Finite-element analysis of unsupported sleepers using three-dimensional wheel–rail contact formulation. *Proc Inst Mech Eng Part K J Multi-body Dyn* 225(2):153–165
15. Zhu JJ, Ahmed AKW, Rakheja S et al (2010) Development of a vehicle–track model assembly and numerical method for simulation of wheel–rail dynamic interaction due to unsupported sleepers. *Veh Syst Dyn* 48(12):1535–1552
16. Li H, Zhao GT, Cai LP (2018) Effects of unsupported sleepers on dynamic response of ballast track structures on bridge. *J Beijing Jiaotong Univ* 42(4):19–26 (in Chinese)
17. Sysyn M, Przybylowicz M, Nabochenko O et al (2021) Identification of sleeper support conditions using mechanical model supported data-driven approach. *Sensors* 21(11):3609
18. Sysyn M, Przybylowicz M, Nabochenko O et al (2021) Mechanism of sleeper–ballast dynamic impact and residual settlements

- accumulation in zones with unsupported sleepers. *Sustainability* 13(14):7740
19. Sysyn M, Nabochenko O, Kovalchuk V (2020) Experimental investigation of the dynamic behavior of railway track with sleeper voids. *Railw Eng Sci* 28(3):290–304
  20. Kim D-S, Kim SD, Lee J (2006) Easy detection and dynamic behavior unsupported sleepers in high speed ballasted track. In: *Proceedings of the seventh world congress on railway research*, paper 414 Montreal, Canada, 4–8 June 2006
  21. Varandas JN, Hölscher P, Silva MAG (2011) Dynamic behavior of railway tracks on transitions zones. *Comput Struct* 89(13–14):1468–1479
  22. Zuada Coelho B, Hicks MA (2016) Numerical analysis of railway transition zones in soft soil. *Proc Inst Mech Eng Part F J Rail Rapid Transit* 230(6):1601–1613
  23. Paixão A, Fortunato E, Calçada R (2015) The effect of differential settlements on the dynamic response of the train-track system: a numerical study. *Eng Struct* 88:216–224
  24. Mosayebi SA, Esmaili M, Zakeri JA (2017) Numerical investigation of the effects of unsupported railway sleepers on train-induced environmental vibrations. *J Low Freq Noise Vib Act Contr* 36(2):160–176
  25. Xu C, Ito K, Hayano K et al (2023) Combined effect of supported and unsupported sleepers on lateral ballast resistance in ballasted railway track. *Transp Geotech* 38:100913
  26. Liu J, Du S, Liu G et al (2023) Influence of unsupported sleepers on the dynamic stability of ballasted bed based on wheelset impact tests. *Railw Eng Sci* 31(1):52–60
  27. Zhang D, Xu P, Tian Y et al (2023) Ballasted track behavior induced by absent sleeper support and its detection based on a convolutional neural network using track data. *Urban Rail Transit* 9(2):92–109
  28. Balamonica K, Bergamini A, Van Damme B (2023) Estimation of the dynamic stiffness of railway ballast over a wide frequency range using the discrete element method. *J Sound Vib* 547:117533
  29. Fang J, Zhao C, Lu X et al (2023) Dynamic behavior of railway vehicle-ballasted track system with unsupported sleepers based on the hybrid DEM-MBD method. *Constr Build Mater* 394:132091
  30. Guo Y, Zhao C, Markine V et al (2020) Discrete element modeling of railway ballast performance considering particle shape and rolling resistance. *Railw Eng Sci* 28(4):382–407
  31. Guo Y, Zhao C, Markine V et al (2020) Calibration for discrete element modeling of railway ballast: a review. *Transp Geotech* 23:100341
  32. Xiao J, Zhang D, Wei K et al (2017) Shakedown behaviors of railway ballast under cyclic loading. *Constr Build Mater* 155:1206–1214
  33. Mansouri P, Zakeri JA, Esmaili M et al (2022) Discrete element method analysis of lateral resistance of different sleepers under different support conditions. *Constr Build Mater* 327:126915
  34. Chalabii J, Movahedi Rad M, Hosseini S (2023) Optimal shape design of concrete sleepers under lateral loading using DEM. *Buildings* 13(7):1574
  35. Guo Y, Fu H, Qian Y et al (2020) Effect of sleeper bottom texture on lateral resistance with discrete element modeling. *Constr Build Mater* 250:118770
  36. Rampat TC, Le Pen L, Powrie W, et al (2019) Evaluating the performance of different sleeper shapes and materials. In: *Railway engineering-2019: 15th International conference & exhibition*. <http://eprints.soton.ac.uk/id/eprint/434411>
  37. Bogacz R, Czyczuła W, Konowrocki R (2014) Influence of sleepers shape and configuration on track-train dynamics. *Shock Vib* 2014:1–7
  38. Wang M, Han X, Jing G et al (2022) Experimental and numerical analysis on mechanical behavior of steel turnout sleeper. *Constr Build Mater* 329:127133
  39. Suhr B, Six K (2022) Efficient DEM simulations of railway ballast using simple particle shapes. *Granul Matter* 24(4):114